Clathrin plaques form mechanotransducing platforms

Agathe Franck[1], Jeanne Lainé[1,2], Gilles Moulay[1], Michaël Trichet[3], Christel Gentil[1], Anaïs Fongy[1], Anne Bigot[1], Sofia Benkhelifa-Ziyyat[1], Emmanuelle Lacène[4], Mai Thao Bui[4], Guy Brochier[4], Pascale Guicheney[5], Vincent Mouly[1], Norma Romero[1,4], Catherine Coirault[1], Marc Bitoun[1] and Stéphane Vassilopoulos[1]*

Affiliations:

[1]Sorbonne Université, INSERM, Institute of Myology, Centre of Research in Myology, UMRS 974, F-75013, Paris, France.

[2]Department of Physiology, Sorbonne Université, UPMC Univ Paris 06, Pitié-Salpêtrière Hospital, Paris, France.

[3]Institut de Biologie Paris-Seine, Sorbonne Université, UPMC Univ Paris 06, CNRS, FR3631, Paris, France.

[4]Neuromuscular Morphology Unit, Institute of Myology, Pitié-Salpêtrière Hospital, Paris, France.

[5]INSERM UMRS_1166, Sorbonne Université, UPMC Univ Paris 06, Institute of Cardiometabolism and Nutrition, Paris, France.

*Corresponding author

Lead contact: Stéphane Vassilopoulos

Sorbonne Université, Inserm U974, Institut de Myologie, Paris, France.

E-mail: s.vassilopoulos@institut-myologie.org

Tel: 33 (0) 1.42.16.57.30

Fax: 33 (0) 1.42.16.57.00

The authors declare no competing financial interests.

Abstract:

Large flat clathrin plaques are stable features of the plasma membrane associated with sites of strong adhesion suggesting that they could also play a role in force transduction. Here, we analyzed how clathrin plaques interact with the cytoskeleton and how they respond to mechanical cues in skeletal muscle myotubes. We show that branched actin networks surrounding clathrin plaques are directly regulated by dynamin 2, anchor intermediate filaments and sequester YAP/TAZ mechanotransducers at the plasma membrane. Dynamin 2, clathrin and desmin intermediate filaments are all required for basal YAP/TAZ nucleo/cytoplasmic distribution and efficient nuclear translocation in response to mechanical stimuli. Dynamin 2 mutations that are responsible for centronuclear myopathy in humans disorganize the desmin network and deregulate YAP/TAZ signaling both *in vitro* and *in vivo*. Thus, clathrin plaques and associated dynamin 2 act as sensors conveying mechanical cues and integrate cell signaling with cytoskeletal regulation.

Introduction

For vesicle formation, clathrin triskelia composed of trimerized heavy chains (CHCs) with bound light chains (CLCs), are recruited by clathrin adaptors that trigger clathrin-coated vesicle (CCV) budding (Brodsky, 2012; Robinson, 2015). The adaptor proteins are required for targeting clathrin to specific intracellular compartments and, among these, adaptor protein 2 (AP2) recruits clathrin to the plasma membrane (PM). In several cell types, and most notably in skeletal muscle myotubes, flat clathrin plaques cover large portions of the PM (Grove et al., 2014; Heuser, 1980; Lampe et al., 2016; Maupin and Pollard, 1983; Saffarian et al., 2009; Taylor et al., 2011). Although flat clathrin lattices are thought to be a structural intermediate which will bud to form a canonical coated pit (Avinoam et al., 2015; Heuser, 1980), the role of these extensive flat clathrin plaques remains elusive. They are invariantly associated with the actin cytoskeleton (Heuser, 1980; Leyton-Puig et al., 2017; Saffarian et al., 2009; Vassilopoulos et al., 2014), they mediate adherence to the extracellular substrate through integrins such as integrin β5 (De Deyne et al., 1998; Lampe et al., 2016; Vassilopoulos et al., 2014) and are thought to serve as hot spots for endocytosis since budding pits are frequently observed at their periphery (Lampe et al., 2016; Taylor et al., 2011). Dynamin 2 (DNM2), a large GTPase which acts as a mechanochemical scaffolding molecule that releases nascent vesicles from the PM or intracellular compartments (van Dam and Stoorvogel, 2002; Kaksonen and Roux, 2018), is a *bona fide* clathrin plaque component (Grove et al., 2014). In addition, several studies have demonstrated that DNM2 regulates actin cytoskeleton networks and have proposed functions for dynamin in actin polymerization that are distinct from coated vesicle formation (Bonazzi et al., 2012; González-Jamett et al., 2017; Gu et al., 2010; Orth and McNiven, 2003; Saffarian et al., 2009; Schafer et al., 2002). Mutations in the *DNM2* gene cause autosomal dominant centronuclear myopathy (CNM) (Bitoun et al., 2005), a slowly progressive congenital

myopathy which is characterized by muscle weakness, hypotonia and the presence of centrally located nuclei in a large number of muscle fibers in the absence of regenerative processes.

In skeletal muscle, CHC and DNM2, are localized at specific PM sites called costameres. CHC depletion *in vivo* leads to drastic detachment of peripheral sarcomeres and decreased force (Cowling et al., 2011; Vassilopoulos et al., 2014). Costameres correspond to lateral contacts between the PM and the contractile apparatus (Pardo et al., 1983b, 1983a; Shear and Bloch, 1985) which play a pivotal role integrating adhesion to the propagation of forces (Danowski et al., 1992). They are composed of large membrane protein complexes, i.e. the focal adhesion complex and the dystrophin-glycoprotein complex that are both linked to the contractile apparatus by actin and desmin intermediate filaments (IFs) (Ervasti, 2003). Desmin is a muscle-specific, type III intermediate filament protein, well documented for its role in cell architecture and force transmission (Capetanaki et al., 2015; Herrmann et al., 2007), which forms a stress-transmitting network involved in signalling, mechanotransduction and gene expression (Palmisano et al., 2015). Costameres are bidirectional mechanochemical signal transduction sites where contractile forces generated within the fiber are directly transmitted to the surrounding extracellular matrix (ECM) and where longitudinal displacement of the ECM is transmitted to the contractile machinery (Samarel, 2005). Although it is established that mechanical cues sensed by costameres are transduced into biochemical signals leading to sarcomeric assembly and gene expression regulation, nothing is known on specific mechanisms involved nor on the role of clathrin plaques and DNM2 at these sites. Two recently identified key mechanotransduction players, Yes-associated protein (YAP) (Sudol, 1994) and Transcriptional co-activator with PDZ-binding motif (TAZ) (Dupont et al., 2011; Kanai et al., 2000), are transcriptional cofactors that can shuttle between the cytoplasm and the nucleus in response to mechanical cues from the ECM (Aragona et al., 2013; Cui et al., 2015; Halder et

al., 2012). Although the precise nature of the compartments that YAP and TAZ associate with in the cytoplasm is unknown, their activity depends on F-actin structures (Aragona et al., 2013).

Here, we set out to investigate the mechanism by which adhesive clathrin plaques could organize a compartment capable of responding to mechanical cues. We report that branched actin filaments around clathrin plaques form signaling platforms for YAP and TAZ and are required to anchor desmin IFs at costameres Alteration of this clathrin-based mechanotransducing platform by *DNM2* mutations which are responsible for CNM highlights a novel pathophysiological mechanism of this congenital myopathy.

Results

Clathrin plaques act as platforms for cytoskeletal organization

We analyzed clathrin plaques from extensively differentiated primary mouse myotubes. Clathrin-positive fluorescent clusters periodically aligned along the PM following organized striated peripheral α-actinin-positive structures (Fig. 1A). We developed a metal-replica electron microscopy (EM) approach aimed at visualizing these structures *en face* from highly differentiated unroofed myotubes. Platinum replicas obtained from both primary mouse (Fig. 1B-D) and human (Supplementary Fig. 5A-C) myotubes presented regularly spaced clathrin plaques interacting with cortical cytoskeletal filaments. Three-dimensional interaction between cytoskeletal components surrounding clathrin plaques was defined by a combination of platinum replica EM and electron tomography by collecting images at the tilt angles up to ±25° with 5° increments relative to the plane of the sample (Supplemental Movie 1). The small clusters of branched actin surrounding clathrin plaques formed a clamp for thicker rope-like filaments weaving through the actin network (Supplementary Fig. 1A, B) and displayed ArpC2 immunogold labeling (Supplementary Fig. 1E, F). Direct visualization and measurements of filament diameter at the ultrastructural level on 3D anaglyphs allowed us to unambiguously discriminate between straight and thin 10 nm on average actin filaments versus thicker 15 nm IFs (including metal coating). Using immunogold labelling combined to metal-replica EM we showed that this three-dimensional network directly connecting actin stress fibers and branched actin "nests" surrounding flat clathrin plaques is composed of desmin IFs (Fig. 1E and Supplementary Fig. 1C, D). We tested the possibility that clathrin plaques were required for organization of the cortical desmin network. CHC depletion in myotubes induced a strong aggregation of desmin in the cytoplasm (Fig. 1F, G). In order to prove that the phenotype was due to clathrin recruited specifically at the PM, we depleted the α-subunit of the AP2 adaptor, which phenocopied CHC depletion and induced the formation of desmin aggregates in the

cytoplasm (Fig. 1G). Importantly, depleting AP1 (γ-subunit) or AP3 (δ-subunit), involved in the recruitment of clathrin to the Golgi apparatus and endosomal systems respectively, had no effect on desmin distribution (Fig. 1G). Thin-section EM confirmed that the aggregates induced by CHC depletion were composed of IF tangles (Fig. 1, H-J). We tested whether desmin was required for clathrin plaque formation by culturing primary myotubes from desmin knock-out mice. These myotubes displayed regularly spaced plaques that were indiscernible from those observed in WT mouse myotubes (Supplementary Fig. 2A). Thus, clathrin plaques and branched actin are necessary for organizing desmin IFs while clathrin plaques can form in the absence of desmin. Altogether, these data demonstrate the importance of clathrin plaques and the surrounding branched actin network for proper organization of the intermediate filament web and suggest that their initial formation is a prerequisite for desmin scaffolding.

Branched actin surrounding clathrin plaques is regulated by N-WASP and DNM2 and organizes desmin intermediate filaments

Neuronal Wiskott–Aldrich Syndrome protein (N-WASP) is directly involved in the generation of Arp2/3 branched actin filaments during endocytosis and a known DNM2 indirect partner (Takenawa and Suetsugu, 2007). N-WASP depletion induced desmin aggregates similar to those produced by CHC depletion (Fig. 2A, C and Supplementary Fig. 4, B-D). DNM2-depleted myotubes displayed particularly pronounced actin defects as demonstrated by phalloidin staining and presented increased cytoplasmic α-actinin 2 (Supplementary Fig. 3A, L) corresponding to dispersed Z-bodies, the precursors of functional sarcomeres (Supplementary Fig. 3B-K). Given DNM2 function in actin remodeling, we reasoned that it could participate to organize branched actin filaments including those surrounding clathrin plaques which anchor intermediate filaments. We observed an interaction between DNM2 and N-WASP and some desmin upon DNM2 immunoprecipitation (Fig. 2F). DNM2-depleted myotubes consistently

displayed increased clathrin patches on the myotube's lateral membrane (Fig. 2B, E and Supplementary Fig. 3A) as well as desmin aggregates in the cytoplasm (Fig. 2B, D, H). At the EM level, both N-WASP and DNM2 depletion produced characteristic actin accumulations associated with additional proteinaceous material (Fig. 2I-K and Supplementary Fig. 4E-H), confirming their requirement for regulating branched F-actin dynamics around clathrin plaques. Overall, we showed the central role played by N-WASP and DNM2 in this unappreciated structural facet of clathrin plaques as organizers of the cortical desmin intermediate filament cytoskeleton.

Clathrin plaques are mechanosensitive platforms and sequestrate YAP/TAZ mechanotransducers via surrounding branched actin structures

Given desmin IFs network function in mechanotransduction, we assessed if clathrin-coated structures (CCS) could respond to mechanical cues. We subjected differentiated myotubes grown on a flexible polydimethylsiloxane (PDMS) substrate to stretching/relaxation cycles. Although metal-replica EM is not compatible with myotubes grown on PDMS, we used a spinning-disc confocal microscope equipped with a super-resolution module with a resolution of 150 nm that is sufficient to distinguish clathrin-coated pits from larger plaques (Fig. 3A). By measuring the size of fluorescently labeled AP2 patches at the surface of myotubes, we observed a significant decrease in plaque size with stretching (Fig. 3B). To test if this size reduction was due to increased clathrin-mediated endocytosis rates, we performed a transferrin uptake assay on cyclically stretched myotubes. Transferrin internalization was significantly increased in cells subjected to a cyclic mechanical strain, reflecting higher rates of clathrin-mediated endocytosis (Fig. 3C). Thus, increased clathrin-mediated endocytosis added to plaque size reduction after stretching demonstrate that clathrin plaques form mechanosensitive structures and suggest that mechanical cues could induce plaque disassembly. Mechanical cues

such as cell stretching cause YAP/TAZ translocation into the nucleus in undifferentiated myoblasts (Fischer et al., 2016). To test YAP/TAZ-mediated cellular responses to mechanical cues in differentiated cells, we subjected myotubes grown on a flexible substrate to cyclic stretching under conditions that would induce translocation of YAP (Cui et al., 2015). At the basal state, YAP/TAZ were mostly cytoplasmic and nuclear staining of both YAP and TAZ increased significantly upon cyclic stretching (Fig. 3D), along an increase in expression of YAP/TAZ canonical target genes *CTGF* and *CYR61* (Fig. 3E). We also noticed an increase of *ACTG1*, coding for γ-actin. To test the contribution of clathrin plaques on YAP and TAZ translocation, we depleted CHC. At the basal state, both YAP and TAZ were strongly accumulated in nuclei from CHC-depleted myotubes (Fig. 3F, G). Consequently, no further nuclear YAP/TAZ increase was observed upon cyclic stretching. Primary myotubes from desmin knock-out mice presented a strong accumulation of YAP in myonuclei at the basal state and no further translocation upon stretching (Supplementary Fig. 2B).

Due to their adhesive nature, we reasoned that clathrin plaques could serve as YAP/TAZ platforms for signaling which could respond to cyclic stretching by increased endocytosis. We used immunogold labeling on metal replicas from unroofed myotubes to specify YAP and TAZ distribution. Both were enriched around plaques as YAP and TAZ associated unambiguously with branched actin filaments located around clathrin-coated plaques and clathrin-coated pits in both mouse and human myotubes (Fig. 3, I-M). Half of all the gold beads were directly associated with clathrin lattices or actin structures ±100 nm away from clathrin lattices (Fig. 3N). We wanted to analyze how they could be retained at these sites. We performed co-immunoprecipitation experiments in primary mouse myotubes to test the interaction between YAP/TAZ and clathrin plaque components such as CHC, DNM2, desmin and N-WASP (Fig. 3H). In agreement with a localization of TAZ directly on clathrin plaques and surrounding actin filaments, we observed a strong interaction between DNM2 and TAZ in differentiated

myotubes suggesting formation of a DNM2/TAZ complex. Altogether, these data suggest that clathrin plaques act as a reservoir for plasmalemmal YAP/TAZ transducers, by their ability to organize a three-dimensional cytoskeletal network around them and that mechanical stimulation induces the releases of YAP/TAZ from the PM via increased endocytosis and subsequent plaque size reduction.

DNM2 is required for YAP/TAZ cytoplasmic sequestration and translocation

We next tested the effect of DNM2 depletion on YAP/TAZ translocation in myotubes. DNM2-depletion phenocopied CHC-depletion and increased YAP in nuclei at the basal state along with an absence of any further response to cyclic stretching (Fig. 4A, C). In contrast, nuclear TAZ levels at the basal state were decreased and these myotubes produced only a marginal translocation of TAZ upon stretching (Fig 4B, D). Acute inhibition of endocytosis using dynamin inhibitor also decreased basal nuclear TAZ levels and responsiveness to stretch (Fig. 4G). Importantly, key YAP/TAZ target genes were highly downregulated in DNM2 depleted myotubes including TAZ itself (Fig. 4, E-F). In addition, DNM2 depletion strongly affected actin genes transcription including γ-actin (Fig. 4E). One particular feature of DNM2 depletion is its strong effect on the actin cytoskeleton. Comparison of filamentous (F) versus globular (G) actin in DNM2 myotubes suggested impairment of F/G actin equilibrium in the cytoplasm of DNM2 depleted myotubes (Supplementary Fig. 3L). MRTF/MKL1, an important mechanotransducer expressed in muscle, translocates out of the nucleus in response to increased G-actin levels and potentiates YAP/TAZ transcriptional activity (Foster et al., 2017; Kim et al., 2017). In agreement with a defect in the F/G actin ratio, MRTF nucleo/cytoplasmic distribution was significantly shifted toward a release of MRTF to the cytoplasm in DNM2-depleted cells (Supplementary Fig. 3M). Altogether, our results suggest that the strong defects produced by DNM2 depletion on the actin cytoskeleton could change the F/G actin ratio and cause MRTF

exit from the nucleus to the cytoplasm which synergizes with an effect on TAZ translocation leading to the reduced expression of canonical YAP/TAZ target genes.

DNM2-linked CNM mutations disorganize TAZ and desmin in vivo and delay plaque dynamics

The association of DNM2 with TAZ and desmin prompted us to analyze their distribution in adult skeletal muscle fibers from wild-type (WT) mice. As for DNM2 and desmin, TAZ presented a characteristic striated distribution at the surface of muscle fibers suggesting a potential role in mechanotransduction adult muscle costameres (Fig. 5, A-B). We applied our mechanistic understanding of DNM2 function in skeletal muscle to the pathophysiology of *DNM2*-related CNM using a knock-in mouse model for the most frequent human mutation, i.e. heterozygous (HTZ) KI-*Dnm2*^{R465W} mice. Given that the AP2 adaptor is specifically recruited at the PM and is a *bona-fide* component of clathrin plaques in muscle (Vassilopoulos et al., 2014), it was used as marker to study the plaques *in vivo*. We transduced the tibialis anterior (TA) muscle with an adeno-associated virus (AAV9) expressing the µ2-subunit of the AP2 clathrin adaptor tagged with mCherry (AP2-mCherry). In WT mice, AP2-mCherry was expressed at the surface of muscle fibers, aligned with the Z-bands and colocalized with endogenous AP2, CHC, DNM2 and α-actinin 2 (Fig. 5C left and Supplementary Fig. 6, A-D left). In HTZ KI-*Dnm2*^{R465W} mice, AP2 distribution was discontinuous and AP2 patches were completely disorganized in the most severely affected regions (Fig. 5C right and Supplementary Fig. 6A-D right). Analysis of muscle from HTZ mice revealed disorganization of TAZ and desmin distribution at the surface of isolated fibers (Fig. 5, D-E). Although TAZ mRNA levels were unchanged, its protein levels were significantly increased in HTZ KI-*Dnm2*^{R465W} mice suggesting increased protein stability (Fig. 5 L).

Our results on the abnormal distribution of AP2 in muscle from HTZ KI-*Dnm2*^{R465W} mice suggesting disorganized clathrin plaques prompted us to analyze their dynamics *in vivo* using intravital microscopy (Fig. 5, F-I). In WT mice, the distribution of AP2 monitored on a kymograph was stable through time, even when imaged at fast acquisition frequencies for periods which exceed the average time that it takes to form an endocytic vesicle (Fig. 5H and Supplemental Movie 2). In addition, *in vivo* AP2 recovery fluorescence recovery after photobleaching (FRAP) was dynamic (Supplemental Movie 3), reaching a 85% plateau in 10 minutes (Fig. 5I) in agreement with *in vitro* experiments (Wu et al., 2003). In HTZ KI-*Dnm2*^{R465W} mice, the speed of fluorescence recovery of AP2 was not significantly delayed, although the plateau only reached 60% (Fig. 5I and Supplemental Movie 4). This decrease in the mobile fraction of AP2 observed in HTZ KI-*Dnm2*^{R465W} mice suggests defective exchange of plaque components.

We next analyzed YAP/TAZ nucleo/cytoplasmic distribution and transcriptional activity in primary myotubes from HTZ KI-*Dnm2*^{R465W} mice. These myotubes display the exact same YAP/TAZ shuttling defects as DNM2-depleted mouse myotubes, with abnormally decreased TAZ nuclear levels at the basal state (Fig. 5K) along with a decreased interaction between DNM2 and TAZ (Fig. 5M). Analysis of immortalized human myotubes cultured from patient expressing the *DNM2* p.R369Q CNM mutation showed a similar pattern, with an increased nuclear YAP at the basal state and no response to cyclic stretching (Supplementary Fig. 5 D-E). Although YAP saturated the nuclei of patient-derived myotubes, expression of its target genes was decreased at the basal state along with a decreased interaction between DNM2 and TAZ (Supplementary Fig. 5, F-G). Expression of YAP/TAZ target genes as well as that of actin isoform genes also mirrored results obtained from DNM2-depleted cells, stressing the importance of DNM2 middle domain in controlling YAP/TAZ signaling and actin transcription (Supplementary Fig. 5G).

We tested whether abnormal desmin organization could contribute to pathological features of CNM. Muscle biopsies from *DNM2*-related CNM patients present a characteristic radial arrangement of sarcoplasmic strands particularly visible with oxidative enzyme reactions. In addition, transverse muscle sections from patients harboring either the p.R465W or the p.R369Q DNM2 mutation presented a strong desmin accumulation in the radiating sarcoplasmic strands, typical of dilated Z-band material, which stretched from central nuclei towards the sarcolemma (Supplementary Fig. 6, E-L).

Discussion

Collectively, our experiments show the existence of a novel compartment centered on clathrin plaques and branched actin which lies at the crossroads of mechanotransduction and cytoskeleton-mediated mechanosensing. We show that actin filaments surrounding mechanically sensitive clathrin plaques sequestrate YAP/TAZ at the membrane and are connected to other parts of the cell by a three-dimensional intermediate filament web. By virtue of shaping both clathrin lattices and branched actin filaments, and by forming a complex with TAZ, DNM2 takes center stage as a YAP/TAZ mechanotransducer and as a regulator of intermediate filaments anchoring.

Comparable to focal adhesions, clathrin plaques are macromolecular functional units that connect extracellular matrix, plasma membrane and intracellular cytoskeleton. Our work shows that branched actin filaments which form around adhesive clathrin plaques are the central element for both IF anchoring and YAP/TAZ recruitment and we identified DNM2 and N-WASP as central actors of actin remodeling at these sites. We have previously shown that the actin network surrounding clathrin lattices contains α-actinin 2, an actin crosslinking protein (Vassilopoulos et al., 2014). The same actin structures require Arp2/3 activity including involvement of the actin nucleation-promoting factor N-WASP in Hela cells (Leyton-Puig et al., 2017). It is of interest that hybrid Arp2/3 and α-actinin containing complexes have already been reported (Chorev et al., 2014; Pizarro-Cerdá et al., 2016) and association of clathrin plaques with these tissue-specific hybrid complexes could be the signature of clathrin's role in adhesion and mechanotransduction. DNM2, previously associated with flat clathrin structures by EM (Damke et al., 1994; Sochacki et al., 2017; Warnock et al., 1997), directly interacts with the cellular machinery, including N-WASP that induces branched actin polymerization around clathrin plaques. We also provide the first evidence that intermediate filaments of desmin, prominent in cells subject to mechanical stress and capable of connecting the cell surface with

peripheral nuclei, are systematically associated with actin structures surrounding clathrin plaques. Depleting either CHC, AP2, N-WASP or DNM2 induced formation of IF aggregates such as those found in patients with desmin mutations (Clemen et al., 2015) demonstrating the strong dependence of the intermediate cytoskeleton organization to the clathrin plaques and associated machinery.

It has been established that in proliferating myoblasts, YAP/TAZ are localized in the nucleus where they act as coactivators for several transcription factors including TEAD factors and promote proliferation (Huang et al., 2005; Lei et al., 2008)(Huang et al., 2005; Lei et al., 2008)(Huang et al., 2005; Lei et al., 2008). During differentiation, both translocate from the nucleus to the cytoplasm thus reducing their transcriptional activity (Watt et al., 2010). In addition, mechanical cues such as cell stretching can cause YAP/TAZ translocation back into the nucleus (Fischer et al., 2016). We show that clathrin plaques and associated cytoskeletal structures might serve as signaling platforms that respond to mechanical cues triggering YAP/TAZ signaling. Metal-replica EM analysis allowed us to unambiguously map YAP and TAZ on actin structures surrounding clathrin plaques suggesting that the same branched actin structures which anchor desmin IFs are also scaffolding YAP and TAZ. Although both YAP and TAZ associated with actin filaments surrounding clathrin plaques, TAZ had a higher propensity to localize close to clathrin-coated structures including budding coated-pits. The interaction between TAZ and DNM2 that we observed in myotubes and the close proximity of their distribution at the surface of adult fibers strengthens the possibility that TAZ distribution depends on DNM2 function. Upon cyclic stretching, i.e. repeated stretching/relaxation cycles, clathrin plaque size was decreased along with an increased clathrin-mediated endocytosis. This endocytosis must occur during the relaxation phases as it has been shown that endocytosis efficiency is inversely correlated to higher membrane tension (Boulant et al., 2011). Our results demonstrate that upon stretching, the plaque size is drastically reduced along a concomitant

YAP/TAZ increase in the nuclei of differentiated myotubes. Taken together, these data strongly suggest that during stretching, endocytosis-mediated remodeling of clathrin plaques releases a pool of YAP and TAZ. Depletion of clathrin, DNM2 and N-WASP resulted in increased nuclear YAP at the basal level of differentiated myotubes. Surprisingly, DNM2 depletion or DNM2-CNM mutants specifically led to decreased TAZ levels and a marginal response to stretching, a phenotype that was reproduced with dynamin inhibitors suggesting endocytosis is required for TAZ translocation. DNM2 function in actin remodeling (González-Jamett et al., 2017; Gu et al., 2010; Orth and McNiven, 2003; Saffarian et al., 2009; Schafer et al., 2002) and one key feature of DNM2 depletion was the strong effect it produced on the actin cytoskeleton. In DNM2 depleted myotubes where a strong disorganization of actin was evident, increased basal nuclear distribution of YAP was accompanied by decreased TAZ levels, decreased transcription of actin genes, including γ-actin which is involved in force transduction and transmission in muscle cells (Craig and Pardo, 1983) and decreased transcription of canonical YAP/TAZ transcriptional targets. Although a decrease in TAZ expression alone could explain the decreased transcription of YAP/TAZ target genes, we show that MRTF/MKL1 nuclear distribution, which has been shown to potentiate YAP/TAZ transcriptional activity, was reduced in DNM2 depleted myotubes. The mutual dependence of MRTF and YAP/TAZ is mediated by cytoskeletal dynamics associated with cell contractility (Foster et al., 2017; Kim et al., 2017). Thus, the strong effect of DNM2 depletion on actin structures induced MRTF translocation into the cytoplasm leading to a decrease in actin and YAP/TAZ target gene expression. Overall, DNM2 appears to function directly at the interface between clathrin plaques and cortical actin network and shapes the actin structures required to anchor intermediate filaments and sequester YAP/TAZ.

DNM2 mutations, causing the autosomal dominant CNM, mostly segregate in the middle domain involved in DNM2 oligomerization and actin remodeling (Durieux et al., 2010;

González-Jamett et al., 2017). This domain has been shown to directly interact with actin, and it is highly probable that the CNM phenotype observed in patients with DNM2 mutations directly stems at least in part from defective cortical actin turnover. These defects in association with the important decrease in actin gene expression observed in CNM patient myotubes would produce dysfunctional force transmission at costameres explaining atrophy and reduced force generation in muscle from the KI-*Dnm2*^{R465W} mouse model (Durieux et al., 2010) in which the F/G actin ratio is altered (González-Jamett et al., 2017). Mechanistic understanding of CNM pathophysiology stemming directly from this work concerns the interplay between nuclear positioning and the IF tangles described here. The link between desmin IFs with both PM and peripheral nuclei in muscle is well established and it was recently shown that Arp2/3 and actin organize desmin for peripheral nuclear positioning (Roman et al., 2017). Our results suggest the peculiar organization termed "radial sarcoplasmic strands", found in CNM patient fibers, is a consequence of the desmin tangles systematically forming at the surface and around nuclei. The desmin tangles could adopt this radiating appearance characteristic of this disease during nuclear centralization. Using the *DNM2*-related CNM knock-in mouse model and patient myotubes we show increased basal nuclear YAP, decreased TAZ and reduced expression of YAP/TAZ target genes corroborating the effect produced by DNM2 depletion and strengthening the link between YAP/TAZ signaling and DNM2 function. It is noteworthy that transgenic mice constitutively expressing nuclear YAP in skeletal muscle displayed a CNM-like phenotype (Judson et al., 2013). Given that desmin defect has been previously identified in the X-linked recessive form of CNM (Hnia et al., 2011), we may hypothesize that desmin IF and YAP/TAZ signaling defects could be a common component of CNM pathophysiology. Further investigation for desmin and YAP/TAZ signaling defects in the autosomal recessive form of CNM due to amphiphysin 2 mutations (Nicot et al., 2007) will be warranted to confirm this common pathophysiological pathway. Importantly, this role may be the Achilles' heel of

several tissues and its dysfunction may lead to additional disorders including cancer where abnormal clathrin plaque assembly could perturb the fine coupling between adhesion and force transduction.

References:

Aragona, M., Panciera, T., Manfrin, A., Giulitti, S., Michielin, F., Elvassore, N., Dupont, S., and Piccolo, S. (2013). A mechanical checkpoint controls multicellular growth through YAP/TAZ regulation by actin-processing factors. Cell *154*, 1047–1059.

Avinoam, O., Schorb, M., Beese, C.J., Briggs, J.A.G., and Kaksonen, M. (2015). Endocytic sites mature by continuous bending and remodeling of the clathrin coat. Science *348*, 1369–1372.

Bitoun, M., Maugenre, S., Jeannet, P.-Y., Lacène, E., Ferrer, X., Laforêt, P., Martin, J.-J., Laporte, J., Lochmüller, H., Beggs, A.H., et al. (2005). Mutations in dynamin 2 cause dominant centronuclear myopathy. Nat. Genet. *37*, 1207–1209.

Bonazzi, M., Kühbacher, A., Toledo-Arana, A., Mallet, A., Vasudevan, L., Pizarro-Cerdá, J., Brodsky, F.M., and Cossart, P. (2012). A common clathrin-mediated machinery co-ordinates cell-cell adhesion and bacterial internalization. Traffic Cph. Den. *13*, 1653–1666.

Boulant, S., Kural, C., Zeeh, J.-C., Ubelmann, F., and Kirchhausen, T. (2011). Actin dynamics counteract membrane tension during clathrin-mediated endocytosis. Nat. Cell Biol. *13*, 1124–1131.

Brodsky, F.M. (2012). Diversity of clathrin function: new tricks for an old protein. Annu. Rev. Cell Dev. Biol. *28*, 309–336.

Capetanaki, Y., Papathanasiou, S., Diokmetzidou, A., Vatsellas, G., and Tsikitis, M. (2015). Desmin related disease: a matter of cell survival failure. Curr. Opin. Cell Biol. *32*, 113–120.

Chorev, D.S., Moscovitz, O., Geiger, B., and Sharon, M. (2014). Regulation of focal adhesion formation by a vinculin-Arp2/3 hybrid complex. Nat. Commun. *5*, 3758.

Clemen, C.S., Stöckigt, F., Strucksberg, K.-H., Chevessier, F., Winter, L., Schütz, J., Bauer, R., Thorweihe, J.-M., Wenzel, D., Schlötzer-Schrehardt, U., et al. (2015). The toxic effect of R350P mutant desmin in striated muscle of man and mouse. Acta Neuropathol. (Berl.) *129*, 297–315.

Cowling, B.S., Toussaint, A., Amoasii, L., Koebel, P., Ferry, A., Davignon, L., Nishino, I., Mandel, J.-L., and Laporte, J. (2011). Increased Expression of Wild-Type or a Centronuclear Myopathy

Mutant of Dynamin 2 in Skeletal Muscle of Adult Mice Leads to Structural Defects and Muscle Weakness. Am. J. Pathol. *178*, 2224–2235.

Craig, S.W., and Pardo, J.V. (1983). Gamma actin, spectrin, and intermediate filament proteins colocalize with vinculin at costameres, myofibril-to-sarcolemma attachment sites. Cell Motil. *3*, 449–462.

Cui, Y., Hameed, F.M., Yang, B., Lee, K., Pan, C.Q., Park, S., and Sheetz, M. (2015). Cyclic stretching of soft substrates induces spreading and growth. Nat. Commun. *6*, 6333.

van Dam, E.M., and Stoorvogel, W. (2002). Dynamin-dependent transferrin receptor recycling by endosome-derived clathrin-coated vesicles. Mol. Biol. Cell *13*, 169–182.

Damke, H., Baba, T., Warnock, D.E., and Schmid, S.L. (1994). Induction of mutant dynamin specifically blocks endocytic coated vesicle formation. J. Cell Biol. *127*, 915–934.

Danowski, B.A., Imanaka-Yoshida, K., Sanger, J.M., and Sanger, J.W. (1992). Costameres are sites of force transmission to the substratum in adult rat cardiomyocytes. J. Cell Biol. *118*, 1411–1420.

De Deyne, P.G., O'Neill, A., Resneck, W.G., Dmytrenko, G.M., Pumplin, D.W., and Bloch, R.J. (1998). The vitronectin receptor associates with clathrin-coated membrane domains via the cytoplasmic domain of its beta5 subunit. J. Cell Sci. *111 (Pt 18)*, 2729–2740.

Dupont, S., Morsut, L., Aragona, M., Enzo, E., Giulitti, S., Cordenonsi, M., Zanconato, F., Le Digabel, J., Forcato, M., Bicciato, S., et al. (2011). Role of YAP/TAZ in mechanotransduction. Nature *474*, 179–183.

Durieux, A.-C., Vignaud, A., Prudhon, B., Viou, M.T., Beuvin, M., Vassilopoulos, S., Fraysse, B., Ferry, A., Lainé, J., Romero, N.B., et al. (2010). A centronuclear myopathy-dynamin 2 mutation impairs skeletal muscle structure and function in mice. Hum. Mol. Genet. *19*, 4820–4836.

Ervasti, J.M. (2003). Costameres: the Achilles' heel of Herculean muscle. J. Biol. Chem. *278*, 13591–13594.

Ezratty, E.J., Bertaux, C., Marcantonio, E.E., and Gundersen, G.G. (2009). Clathrin mediates integrin endocytosis for focal adhesion disassembly in migrating cells. J. Cell Biol. *187*, 733–747.

Falcone, S., Roman, W., Hnia, K., Gache, V., Didier, N., Lainé, J., Auradé, F., Marty, I., Nishino, I., Charlet-Berguerand, N., et al. (2014). N-WASP is required for Amphiphysin-2/BIN1-dependent

nuclear positioning and triad organization in skeletal muscle and is involved in the pathophysiology of centronuclear myopathy. EMBO Mol. Med. *6*, 1455–1475.

Fischer, M., Rikeit, P., Knaus, P., and Coirault, C. (2016). YAP-Mediated Mechanotransduction in Skeletal Muscle. Front. Physiol. *7*, 41.

Foster, C.T., Gualdrini, F., and Treisman, R. (2017). Mutual dependence of the MRTF-SRF and YAP-TEAD pathways in cancer-associated fibroblasts is indirect and mediated by cytoskeletal dynamics. Genes Dev. *31*, 2361–2375.

González-Jamett, A.M., Baez-Matus, X., Olivares, M.J., Hinostroza, F., Guerra-Fernández, M.J., Vasquez-Navarrete, J., Bui, M.T., Guicheney, P., Romero, N.B., Bevilacqua, J.A., et al. (2017). Dynamin-2 mutations linked to Centronuclear Myopathy impair actin-dependent trafficking in muscle cells. Sci. Rep. *7*, 4580.

Grove, J., Metcalf, D.J., Knight, A.E., Wavre-Shapton, S.T., Sun, T., Protonotarios, E.D., Griffin, L.D., Lippincott-Schwartz, J., and Marsh, M. (2014). Flat clathrin lattices: stable features of the plasma membrane. Mol. Biol. Cell *25*, 3581–3594.

Gu, C., Yaddanapudi, S., Weins, A., Osborn, T., Reiser, J., Pollak, M., Hartwig, J., and Sever, S. (2010). Direct dynamin-actin interactions regulate the actin cytoskeleton. EMBO J. *29*, 3593–3606.

Halder, G., Dupont, S., and Piccolo, S. (2012). Transduction of mechanical and cytoskeletal cues by YAP and TAZ. Nat. Rev. Mol. Cell Biol. *13*, 591–600.

Herrmann, H., Bär, H., Kreplak, L., Strelkov, S.V., and Aebi, U. (2007). Intermediate filaments: from cell architecture to nanomechanics. Nat. Rev. Mol. Cell Biol. *8*, 562–573.

Heuser, J. (1980). Three-dimensional visualization of coated vesicle formation in fibroblasts. J. Cell Biol. *84*, 560–583.

Heuser, J. (2000). The production of "cell cortices" for light and electron microscopy. Traffic Cph. Den. *1*, 545–552.

Hnia, K., Tronchère, H., Tomczak, K.K., Amoasii, L., Schultz, P., Beggs, A.H., Payrastre, B., Mandel, J.L., and Laporte, J. (2011). Myotubularin controls desmin intermediate filament architecture and mitochondrial dynamics in human and mouse skeletal muscle. J. Clin. Invest. *121*, 70–85.

Huang, J., Wu, S., Barrera, J., Matthews, K., and Pan, D. (2005). The Hippo Signaling Pathway Coordinately Regulates Cell Proliferation and Apoptosis by Inactivating Yorkie, the Drosophila Homolog of YAP. Cell *122*, 421–434.

Judson, R.N., Gray, S.R., Walker, C., Carroll, A.M., Itzstein, C., Lionikas, A., Zammit, P.S., Bari, C.D., and Wackerhage, H. (2013). Constitutive Expression of Yes-Associated Protein (Yap) in Adult Skeletal Muscle Fibres Induces Muscle Atrophy and Myopathy. PLOS ONE *8*, e59622.

Kaksonen, M., and Roux, A. (2018). Mechanisms of clathrin-mediated endocytosis. Nat. Rev. Mol. Cell Biol.

Kanai, F., Marignani, P.A., Sarbassova, D., Yagi, R., Hall, R.A., Donowitz, M., Hisaminato, A., Fujiwara, T., Ito, Y., Cantley, L.C., et al. (2000). TAZ: a novel transcriptional co-activator regulated by interactions with 14-3-3 and PDZ domain proteins. EMBO J. *19*, 6778–6791.

Kim, T., Hwang, D., Lee, D., Kim, J.-H., Kim, S.-Y., and Lim, D.-S. (2017). MRTF potentiates TEAD-YAP transcriptional activity causing metastasis. EMBO J. *36*, 520–535.

Kirchhausen, T. (1999). Adaptors for clathrin-mediated traffic. Annu. Rev. Cell Dev. Biol. *15*, 705–732.

Lampe, M., Vassilopoulos, S., and Merrifield, C. (2016). Clathrin coated pits, plaques and adhesion. J. Struct. Biol. *196*, 48–56.

Lei, Q.-Y., Zhang, H., Zhao, B., Zha, Z.-Y., Bai, F., Pei, X.-H., Zhao, S., Xiong, Y., and Guan, K.-L. (2008). TAZ Promotes Cell Proliferation and Epithelial-Mesenchymal Transition and Is Inhibited by the Hippo Pathway. Mol. Cell. Biol. *28*, 2426–2436.

Leyton-Puig, D., Isogai, T., Argenzio, E., van den Broek, B., Klarenbeek, J., Janssen, H., Jalink, K., and Innocenti, M. (2017). Flat clathrin lattices are dynamic actin-controlled hubs for clathrin-mediated endocytosis and signalling of specific receptors. Nat. Commun. *8*, 16068.

Maupin, P., and Pollard, T.D. (1983). Improved preservation and staining of HeLa cell actin filaments, clathrin-coated membranes, and other cytoplasmic structures by tannic acid-glutaraldehyde-saponin fixation. J. Cell Biol. *96*, 51–62.

Nicot, A.-S., Toussaint, A., Tosch, V., Kretz, C., Wallgren-Pettersson, C., Iwarsson, E., Kingston, H., Garnier, J.-M., Biancalana, V., Oldfors, A., et al. (2007). Mutations in amphiphysin 2 (BIN1)

disrupt interaction with dynamin 2 and cause autosomal recessive centronuclear myopathy. Nat. Genet. *39*, 1134–1139.

Orth, J.D., and McNiven, M.A. (2003). Dynamin at the actin-membrane interface. Curr. Opin. Cell Biol. *15*, 31–39.

Palmisano, M.G., Bremner, S.N., Hornberger, T.A., Meyer, G.A., Domenighetti, A.A., Shah, S.B., Kiss, B., Kellermayer, M., Ryan, A.F., and Lieber, R.L. (2015). Skeletal muscle intermediate filaments form a stress-transmitting and stress-signaling network. J. Cell Sci. *128*, 219–224.

Pardo, J.V., Siliciano, J.D., and Craig, S.W. (1983b). A vinculin-containing cortical lattice in skeletal muscle: transverse lattice elements ("costameres") mark sites of attachment between myofibrils and sarcolemma. Proc. Natl. Acad. Sci. U. S. A. *80*, 1008–1012.

Pardo, J.V., Siliciano, J.D., and Craig, S.W. (1983a). Vinculin is a component of an extensive network of myofibril-sarcolemma attachment regions in cardiac muscle fibers. J. Cell Biol. *97*, 1081–1088.

Pearse, B.M., and Robinson, M.S. (1990). Clathrin, adaptors, and sorting. Annu. Rev. Cell Biol. *6*, 151–171.

Pizarro-Cerdá, J., Chorev, D.S., Geiger, B., and Cossart, P. (2016). The Diverse Family of Arp2/3 Complexes. Trends Cell Biol.

Rivière, C., Danos, O., and Douar, A.M. (2006). Long-term expression and repeated administration of AAV type 1, 2 and 5 vectors in skeletal muscle of immunocompetent adult mice. Gene Ther. *13*, 1300–1308.

Robinson, M.S. (2015). Forty Years of Clathrin-coated Vesicles. Traffic Cph. Den. *16*, 1210–1238.

Roman, W., Martins, J.P., Carvalho, F.A., Voituriez, R., Abella, J.V.G., Santos, N.C., Cadot, B., Way, M., and Gomes, E.R. (2017). Myofibril contraction and crosslinking drive nuclear movement to the periphery of skeletal muscle. Nat. Cell Biol. *19*, 1189–1201.

Saffarian, S., Cocucci, E., and Kirchhausen, T. (2009). Distinct dynamics of endocytic clathrin-coated pits and coated plaques. PLoS Biol. *7*, e1000191.

Samarel, A.M. (2005). Costameres, focal adhesions, and cardiomyocyte mechanotransduction. Am. J. Physiol. Heart Circ. Physiol. *289*, H2291-2301.

Schafer, D.A., Weed, S.A., Binns, D., Karginov, A.V., Parsons, J.T., and Cooper, J.A. (2002). Dynamin2 and cortactin regulate actin assembly and filament organization. Curr. Biol. CB *12*, 1852–1857.

Schindelin, J., Arganda-Carreras, I., Frise, E., Kaynig, V., Longair, M., Pietzsch, T., Preibisch, S., Rueden, C., Saalfeld, S., Schmid, B., et al. (2012). Fiji: an open-source platform for biological-image analysis. Nat. Methods *9*, 676–682.

Shear, C.R., and Bloch, R.J. (1985). Vinculin in subsarcolemmal densities in chicken skeletal muscle: localization and relationship to intracellular and extracellular structures. J. Cell Biol. *101*, 240–256.

Sochacki, K.A., Dickey, A.M., Strub, M.-P., and Taraska, J.W. (2017). Endocytic proteins are partitioned at the edge of the clathrin lattice in mammalian cells. Nat. Cell Biol. *19*, 352–361.

Sudol, M. (1994). Yes-associated protein (YAP65) is a proline-rich phosphoprotein that binds to the SH3 domain of the Yes proto-oncogene product. Oncogene *9*, 2145–2152.

Takenawa, T., and Suetsugu, S. (2007). The WASP-WAVE protein network: connecting the membrane to the cytoskeleton. Nat. Rev. Mol. Cell Biol. *8*, 37–48.

Taylor, M.J., Perrais, D., and Merrifield, C.J. (2011). A high precision survey of the molecular dynamics of mammalian clathrin-mediated endocytosis. PLoS Biol. *9*, e1000604.

Vassilopoulos, S., Gentil, C., Lainé, J., Buclez, P.-O., Franck, A., Ferry, A., Précigout, G., Roth, R., Heuser, J.E., Brodsky, F.M., et al. (2014). Actin scaffolding by clathrin heavy chain is required for skeletal muscle sarcomere organization. J. Cell Biol. *205*, 377–393.

Warnock, D.E., Baba, T., and Schmid, S.L. (1997). Ubiquitously expressed dynamin-II has a higher intrinsic GTPase activity and a greater propensity for self-assembly than neuronal dynamin-I. Mol. Biol. Cell *8*, 2553–2562.

Watt, K.I., Judson, R., Medlow, P., Reid, K., Kurth, T.B., Burniston, J.G., Ratkevicius, A., De Bari, C., and Wackerhage, H. (2010). Yap is a novel regulator of C2C12 myogenesis. Biochem. Biophys. Res. Commun. *393*, 619–624.

Wu, X., Zhao, X., Puertollano, R., Bonifacino, J.S., Eisenberg, E., and Greene, L.E. (2003). Adaptor and clathrin exchange at the plasma membrane and trans-Golgi network. Mol. Biol. Cell *14*, 516–528.

Materials and methods:

Antibodies

Primary antibodies are listed in Supplementary Table 3. Secondary antibodies for immunofluorescence were AlexaFluor-488, AlexaFluor-568 and AlexaFluor-647 conjugates (Life Technologies, France). Secondary antibodies were coupled to horseradish peroxidase (Jackson Laboratories, USA). Secondary antibodies used after immunoprecipitation were Trueblot IgG HRP from Rockland Inc., USA.

Human myoblast cultures

Immortalized control and patient myoblast cells (DNM2 p.R369Q) were cultured in proliferation medium (1 volume of M199, #41150020, Invitrogen, France), 4 volumes of DMEM Glutamax, 20% fetal bovine serum (FBS), 50 U/mL penicillin, 50 mg/mL streptomycin, 25 µg/mL fetuin (#10344026; Life Technologies, France), 0.5 ng/mL fibroblast growth factor-basic (bFGF; #PHG0026; Life Technologies, France), 5 ng/mL human epidermal growth factor (hEGF; #PHG0311; Life Technologies, France), 0.2 µg/mL dexamethasone (#D4902-100mg; Sigma, France), 5 µg/mL insulin (#91077C-1g; Sigma, France). Differentiation was induced using DMEM Glutamax, 2% Horse Serum, 50 U/mL penicillin, 50 mg/mL streptomycin, supplemented with 5µg/mL insulin (#91077C-1G; Sigma, France).

Mouse myoblast cultures and siRNA-mediated knock-down

Primary skeletal muscle cells were prepared from 3-4 day-old mouse pups. Cells were maintained in tissue culture dishes coated with Matrigel Matrix (Corning, France) in basal medium with 20% FBS, 50 U/mL penicillin, 50 mg/mL streptomycin (growth medium) and 1% Chicken Embryo Extract (Seralab, UK). Differentiation was induced when cells were ~80% confluent by switching to differentiation medium (basal medium with 2% horse serum). For

experiments in Figure 1, in order to avoid detachment due to strong contractions, and to keep cells in culture for prolonged periods of differentiation, myotubes were covered with a layer of Matrigel Growth Factor Reduced (GFR) Basement Membrane Matrix, Phenol Red-Free (Corning, France) (Falcone et al., 2014). For siRNA treatment, cells (differentiated for either 4 or 6 days) were transfected twice for 48 hours using 200 nM siRNA and HiPerfect transfection reagent (Qiagen, Germany) according to manufacturer's instructions. Targeting and control siRNAs were synthesized by Eurogentec, Belgium. The list of siRNAs used and sequences can be found in Supplementary Table 2. For CHC, AP2 and DNM2, sequences targeted were already published (Ezratty et al., 2009; Vassilopoulos et al., 2014).

Electron microscopy of unroofed myotubes

Adherent PM from cultured cells grown on glass coverslips were obtained by sonication as described previously (Heuser, 2000). Sample processing for platinum-replica electron microscopy of unroofed cells was performed as follows: 2% glutaraldehyde/ 2% paraformaldehyde-fixed cells were further sequentially treated with 1% OsO4, 1% tannic acid and 1% uranyl acetate prior to graded ethanol dehydration and Hexamethyldisilazane (HMDS) (Sigma-Aldrich, France). For immunogold labeling, 4% paraformaldehyde fixed PMs were washed and quenched before incubation with primary and 15nm gold-coupled secondary antibodies and further fixed with 2% glutaraldehyde. Dried samples were then rotary-shadowed with 2 nm of platinum and 5-8 nm of carbon using an ACE600 metal coater (Leica Microsystems, Germany). The resultant platinum replica was floated off the glass with hydrofluoric acid (5%), washed several times on distilled water, and picked up on 200 mesh formvar/carbon-coated EM grids. The grids were mounted in a eucentric side-entry goniometer stage of a transmission electron microscope operated at 80 kV (model CM120; Philips) and images were recorded with a Morada digital camera (Olympus, Tokyo). Images were processed

in Adobe Photoshop to adjust brightness and contrast and presented in inverted contrast. Anaglyphs were made by converting the -10° tilt image to red and the +10° tilt image to cyan (blue/green), layering them on top of each other using the screen blending mode in Adobe Photoshop, and aligning them to each other. Tomograms were made by collecting images at the tilt angles up to ±25° relative to the plane of the sample with 5° increments. Images were aligned by layering them on top of each other in Adobe Photoshop.

Dissociated fibers

Myofibers were isolated by mechanical dissociation from the dissected *tibialis anterior* (TA) muscle of 3-month old or 7-month old mice fixed 48 hours in 4% paraformaldehyde.

Immunofluorescence microscopy

Adult mouse skeletal muscle was embedded in Tissue-Tek OCT compound (Miles Inc.), frozen, and stored at -80°C. Cryosections (10 µm thick) were fixed (15 min, 4% paraformaldehyde in PBS) at room temperature (RT), permeabilized (10 min, 0.5% Triton X-100 in PBS, RT) and blocked (30 min, PBS with 0.1% Triton X-100, 5% bovine serum albumin (BSA). Sections were incubated with primary antibodies (overnight, 4°C, in PBS with 0.1% Triton X-100, 5% BSA) and washed in PBS with 0.1% Triton X-100. Sections were then incubated with secondary antibodies (60 min, RT), washed in PBS with 0.1% Triton X-100, and mounted with Vectashield anti-fading solution containing DAPI (Vector Laboratories, USA). For double or triple labeling, the primary antibodies (from different species) were added simultaneously at the appropriate step.

For mouse cells grown on coverslips, cells were washed in warm PBS, fixed in paraformaldehyde (4% in PBS, 15 min), then washed in PBS, permeabilized (10 min, 0.5% Triton X-100 in PBS) and blocked (5% BSA in PBS with 0.1% Triton X-100, 30 min).

Antibody labeling was performed by addition of 200 µL blocking solution with primary or secondary antibodies and washing with PBS with 0.1% Triton X-100. F-Actin was stained using Alexa Fluor 555 Phalloidin and G-actin was stained using Alexa 488 DNase I (Thermo Fisher Scientific, France) for 1h at RT. Samples were mounted in Vectashield containing DAPI (Vector Laboratories, USA).

Samples were analyzed by confocal laser scanning microscopy using an upright FV-1000 confocal laser scanning microscope (Olympus, Tokyo) equipped with UPlanS-Apo 60x, 1.35 NA oil immersion objective lenses or a SP5 inversed microscope (Leica, Germany) equipped with a Leica HyD hybrid detector. Super resolution spinning-disk confocal images presented in Fig. 3A were taken with a Nikon Ti2 microscope equipped with a motorized stage and a Yokogawa CSU-W1 spinning disk head coupled with a Prime 95 sCMOS camera (Photometrics). To obtain super resolutive images, a Live SR module (Roper) was used. DAPI, Alexa-488 and Alexa-568 were sequentially excited using lasers with wavelengths of 405 for DAPI, 473 for Alexa-488 and 543 nm for Alexa-568. Z-series from the top to the bottom of fibers were sequentially collected for each channel with a step of 0.8-1µm between each frame. Imaging was performed at RT using Leica Type F immersion oil. Images (1024 × 1024 pixels) were saved as TIFF files in OLYMPUS FV-1000 software, and levels were adjusted in Adobe Photoshop or Gimp software. Image quantification was performed using National Institutes of Health's FIJI (Schindelin et al., 2012).

Cyclic stretch

Cells were plated onto flexible-bottom UniFlex or BioFlex plates (Flexcell International, USA) coated with Corning Matrigel GFR Basement Membrane Matrix and incubated at 37°C in a CO_2 incubator. The cells were subjected to cyclic stretch at 0.5 Hz during 6 hours using a computer-controlled vacuum FX-4000T Tension Plus System stretch apparatus (FlexCell

International, USA) with a vacuum pressure that is sufficient to generate 10% mechanical stretch. Replicate control samples were maintained under static conditions with no applied cyclic stretch. After stretching, cells were washed with PBS and fixed using 4% paraformaldehyde for immunofluorescence, NaCl-EDTA buffer for western blotting or TRIzol reagent (Life Technologies, USA) for gene analysis.

Transferrin assay

Cells were subjected to cyclic stretching for 4 hours with or without 80 µM Dynasore (Sigma-Aldrich, France) before incubation 15 min with AlexaFluor-488 fluorescently labeled human transferrin (40 µg/mL) (Molecular Probes, Life Technologies, France) concomitant to stretching. Endocytosis of this compound was stopped with ice-cold PBS washing and fixed using 4% paraformaldehyde.

Entire myotubes were images using stacks of 500 nm step, with an FV-1200 confocal microscope (Olympus, Tokyo) and 40x oil objective. Experiment was performed twice with similar results.

Immunoblot analysis

Cell samples were collected using Laemli blue 4X directly or a NaCl (150 mM)-EDTA (10 mM) buffer with added proteinase inhibitor cocktail (Sigma-Aldrich, France).

Protein samples were separated by electrophoresis (4-12% bis-acrylamide gel, Life Technologies, France), then electrophoretically transferred to 0.45 µm nitrocellulose membranes (Life Technologies, France) and labelled with primary antibodies and secondary antibodies coupled to horseradish peroxidase. The presence of proteins in samples was detected using Immobilon Western Chemiluminescent HRP Substrate (Sigma-Alrich, France). Acquisition was performed on a G-Box (Ozyme, France).

Immunoprecipitation

IPs were performed on primary cell cultures. Myotube pellets were resuspended in 500 µL of lysis buffer (50 mM Tris-HCl, pH 7.5, 0.15 M NaCl, 1 mM EDTA, 1% NP-40) and protein inhibitor cocktail 1:100 (Sigma Aldrich, France). Each sample (200-500 µg) was precleared twice with 30 µL Protein-G-Sepharose (PGS 4 fast flow, Thermo Fisher, France) and incubated with 20 µg of specific antibody overnight (4°C). Washed PGS (40 µL) was first incubated with BSA (2 g/L) and further incubated with samples for 2 hours at 4°C. Pelleted PGS was taken up in sample buffer and subjected to electrophoresis and immunoblotting. For all immunoprecipitation experiments, HRP-conjugated rabbit and mouse IgG TrueBlot secondary antibodies (Rockland Inc., USA) were used.

Intravital-imaging

WT and HTZ KI-Dnm2^{R465W} mice (Durieux et al., 2010) injected a month prior with AAV-µ2-mCherry were anesthetized using isofluorane. Skin was removed from the TA before applying muscle directly on coverslip and immobilizing with tape (Figure 5F). Imaging and FRAP was performed on an inverted Leica SP8 multiphoton microscope optimized for intravital microscopy of small animals, equipped with a complete isofluorane anesthesia unit. The mouse temperature was maintained at 37°C with a heating stage and a heating lamp, and breathing of the animal was monitored visually throughout the experiment.

AAV production, titration and *in vivo* gene transfer

An adeno-associated virus serotype 9 was produced for expression of the µ2-subunit of the AP2 clathrin adaptor tagged with mCherry (AP2-mCherry) (Taylor et al., 2011). AAV2/9 pseudotyped vectors were prepared by tri-transfection in 293 cells as described previously

(Rivière et al., 2006) using the pSMD2-AP2-mCherry plasmid, pXX6 plasmid coding for the viral sequences essential for AAV production and the pRepCap plasmid coding for serotype 9 capsid. Vector particles were purified on iodixanol gradient and concentrated on Amicon Ultra-15 100K columns (Merck-Millipore, USA). The viral genomes titer (vg/mL) was determined by quantitative real-time PCR. WT and HTZ KI-Dnm2^{R465W} mice were injected at 6 months of age. One intramuscular injection (40 µL/TA) of AAV9-AP2-mCherry was performed in TA muscles using 29G needle.

Histomorphological and ultrastructural analyses

Human open muscle biopsies from two patients carrying the CNM-dynamin-2 mutation p.R465W, one patient carrying the CNM-dynamin-2 mutation p.R369Q, and one healthy control muscle were performed at the Centre de Référence de Pathologie Neuromusculaire Paris-Est, Institut de Myologie, GHU Pitié-Salpêtrière, Assistance Publique-Hôpitaux de Paris, GH Pitié-Salpêtrière, Paris, France, following written informed consent specially dedicated for diagnosis and research. Muscle was frozen in liquid nitrogen-cooled isopentane. Transverse and longitudinal muscle sections were stained and analyzed by confocal laser scanning microscopy using an upright FV-1000 confocal microscope (Olympus, Tokyo) as previously described. For all imaging, exposure settings were identical between compared samples and viewed at room temperature. For conventional histochemical techniques on human biopsies, 10 µm thick cryostat sections were stained with antibodies against desmin or with reduced nicotinamide adenine dinucleotide dehydrogenase-tetrazolium reductase (NADH-TR) by standard methods. Pictures of each section were obtained with a Zeiss AxioCam HRc linked to a Zeiss Axioplan Bright Field Microscope and processed with the Axio Vision 4.4 software (Zeiss, Germany).

For thin-section EM, mouse muscles were fixed by intra-aortic perfusion with 2% paraformaldehyde, 2% glutaraldehyde in 0.1M phosphate buffer (pH 7.4). Tibialis anterior samples were postfixed with 2% OsO4, in 0.1 M phosphate buffer (pH 7.4) for 1 h, then dehydrated in a graded series of acetone including a 1% uranyl acetate staining step in 70% acetone, and finally embedded in epoxy resin (EMBed-812, Electron Microscopy Sciences, USA). Myotubes grown on Thermanox coverslips (Nunc, Rochester, USA) were directly fixed for 30 min in the same fixation solution and processed as previously indicated for tibialis anterior muscles. Ultra-thin (70 nm) sections were stained with uranyl acetate and lead citrate. For patient biopsies, frozen muscle sections (40 µm) were fixed in osmium tetroxide (1%), dehydrated and embedded in epoxy resin (as above). Ultra-thin (80 nm) sections were stained with uranyl acetate and lead citrate. Observations were made on a Philips CM120 electron microscope operated at 80kV (Philips, Eindhoven, The Netherlands) and images were recorded with a Morada digital camera (Olympus Soft Imaging Solutions GmbH, Münster, Germany).

RNA extraction and RT-qPCR

RNAs were isolated from TA muscles or from myotubes either four days after siRNA transfection, or right after the end of the stretching period, using TRIzol reagent (Life Technologies, USA) according to the manufacturer's protocol. Total RNA was then submitted to a DNaseI treatment (New England Biolabs, USA) followed by a phenol-chloroform extraction, and stored at -80°C following Nanodrop ND-1000 spectrophotometer quantification (Nanodrop Technologies, USA). 1 µg of RNA was reverse transcribed using M-MLV first-strand synthesis system according to the manufacturer's instructions (Invitrogen, USA) in a total of 20 µL.

To quantify the mRNA expression, real-time PCR was performed using a Lightcycler 480 II (Roche, Switzerland) and 1X SYBR Green (Roche, Switzerland) reactions using 0.2 pmol/µL

of forward and reverse primer, and 5 µL of each cDNA diluted to at 1:10 in nuclease-free water. PCR primer sequences for both human and mouse cDNA are listed in Supplementary Table 1. PCR cycles were a 10 min 95°C pre-incubation step followed by 45 cycles with a 95°C denaturation for 10 s, 60°C annealing for 15 s and 72°C extension for 8 s. Each target expression level was normalized using RPLP0 and HPRT1 geometric mean. The quantitative data are the means ± SEM of two to three independent experiments cumulating respectively n = 6-8 and n = 2-4 samples for Fig. 4E and Supplementary Fig. 5G. Statistical significance was defined by a Student T-test with two-tailed p-value below 0.05.

Image analysis

Desmin aggregate size analysis: the "Analyze particles" FIJI plugin (version 1.46) was used to count intracellular particles on binary confocal images of primary mouse myotubes in a single image from the middle of the cell. Same treatment was performed to measure the size of clathrin plaques on confocal images. Transferrin-A488 fluorescence was measured on confocal images by selecting 5 ROIs in myotubes, background noise, and using this formula: CTCF = Integrated density – (Area of selected cell X Mean fluorescence of background reading). FRAP analysis: Drifting was corrected using FIJI plugin JavaSIFT. Intensity of bleached area was compared to overall intensity of the muscle fiber, frame by frame, using FRAP Profiler plugin for FIJI.

Statistics and institutional guideline compliance

Statistical analysis was performed using Student's t-test except as otherwise stated.

Study approval

Animal studies conform to the French laws and regulations concerning the use of animals for research and were approved by an external Ethical committee (approval n°00351.02 delivered by the French Ministry of Higher Education and Scientific Research).

For human studies, all individuals provided informed consent for muscle biopsies according to a protocol approved by the ethics committee of the Centre de Référence de Pathologie Neuromusculaire Paris-Est, Institut de Myologie, GHU Pitié-Salpêtrière, Assistance Publique-Hôpitaux de Paris, GH Pitié-Salpêtrière, Paris, France.

Data availability

All data supporting the findings of this study are available from the corresponding authors on request.

Author contributions:

A.Fr., J.L. and M.B., designed and performed experiments, analyzed results and wrote the manuscript. G.M., M.T., C.G., A.Fo., S.B-Z., A.B., E.L., M.T.B., G.B. performed experiments. G.M., V.M., P.G., N.R., and C.C. analyzed the data. S.V supervised the study, designed and performed experiments and wrote the manuscript. All authors read and approved the final version of the manuscript.

Acknowledgements:

We are grateful to John Heuser and Azumi Yoshimura for precious help throughout this work. We dedicate this work to the memory of our friend Christien Merrifield. We also thank Onnik Agbulut for reagents, advices and comments, the Penn Vector Core, Gene Therapy Program (University of Pennsylvania, Philadelphia, US) for providing the plasmids for AAV construction, Laura Julien for AAV production, the Pitié-Salpêtrière (PICPS) and the Gustave

Roussy institute imaging platforms for confocal and two-photon imaging facilities respectively and the IBPS electron microscopy platform. This work was supported by the Institut National de la Santé et de la Recherche Médicale (INSERM), Association Institut de Myologie (AIM), Sorbonne Université (SU), Centre National de la Recherche Scientifique (CNRS), an Agence Nationale de la Recherche grant (ANR-14-CE12-0009 Dynamuscle) to M.B. and a young researcher grant (ANR-14-CE12-0001-01 Endomechano) to S.V.

Figures:

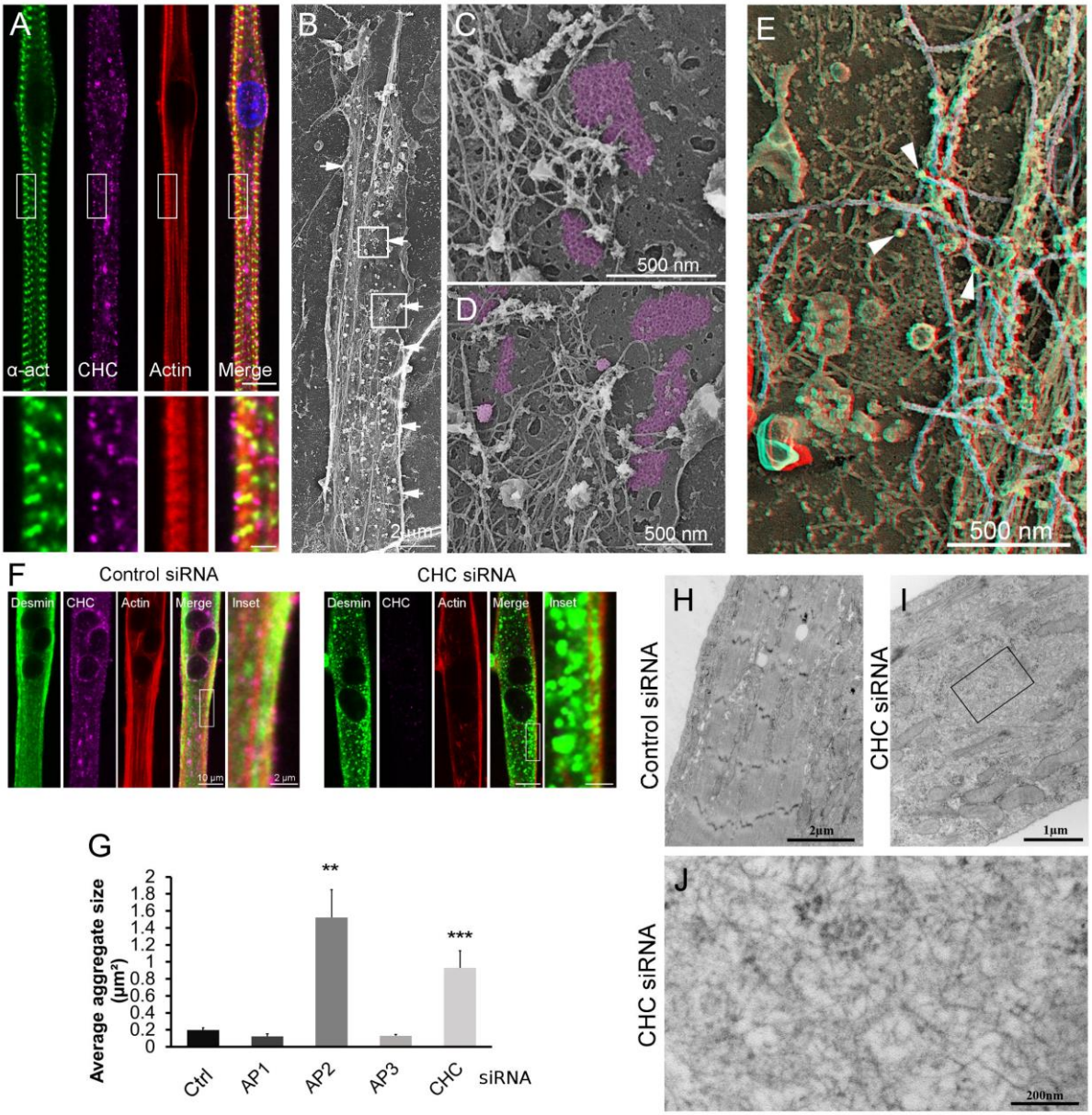

Fig. 1. Clathrin-coated plaques are required for intermediate filament organization. (A) Immunofluorescent staining of α-actinin 2 (green), CHC (magenta), and actin (red) in extensively differentiated mouse primary myotubes. Bars are 10 µm and 2 µm for insets. **(B)** Survey view of unroofed primary mouse myotube differentiated for 15 days. **(C) (D)** Higher magnification views corresponding to the boxed regions in b. **(E)** Unroofed control primary myotubes were labelled with desmin antibodies (pseudocolored yellow, arrowheads). Intermediate filaments are highlighted in grey. Use glasses for 3D viewing of anaglyph (left eye = red). **(F)** Immunofluorescent staining of desmin (green), CHC (magenta) and actin (red) in mouse primary myotubes treated with control (left) siRNA or siRNA against CHC (right). **(G)** Average desmin aggregate size in myotubes treated with control siRNA or siRNA against CHC, AP1, AP2 or AP3 (n = 30–50 myotubes. Data presented as mean ± SEM; **P < 0.01, ***P < 0.001, ****P < 0.0001). **(H) (I)** Thin-section EM of primary myotubes treated with control (e) or CHC (f) siRNA. **(J)** Higher magnification view of desmin tangles from (I).

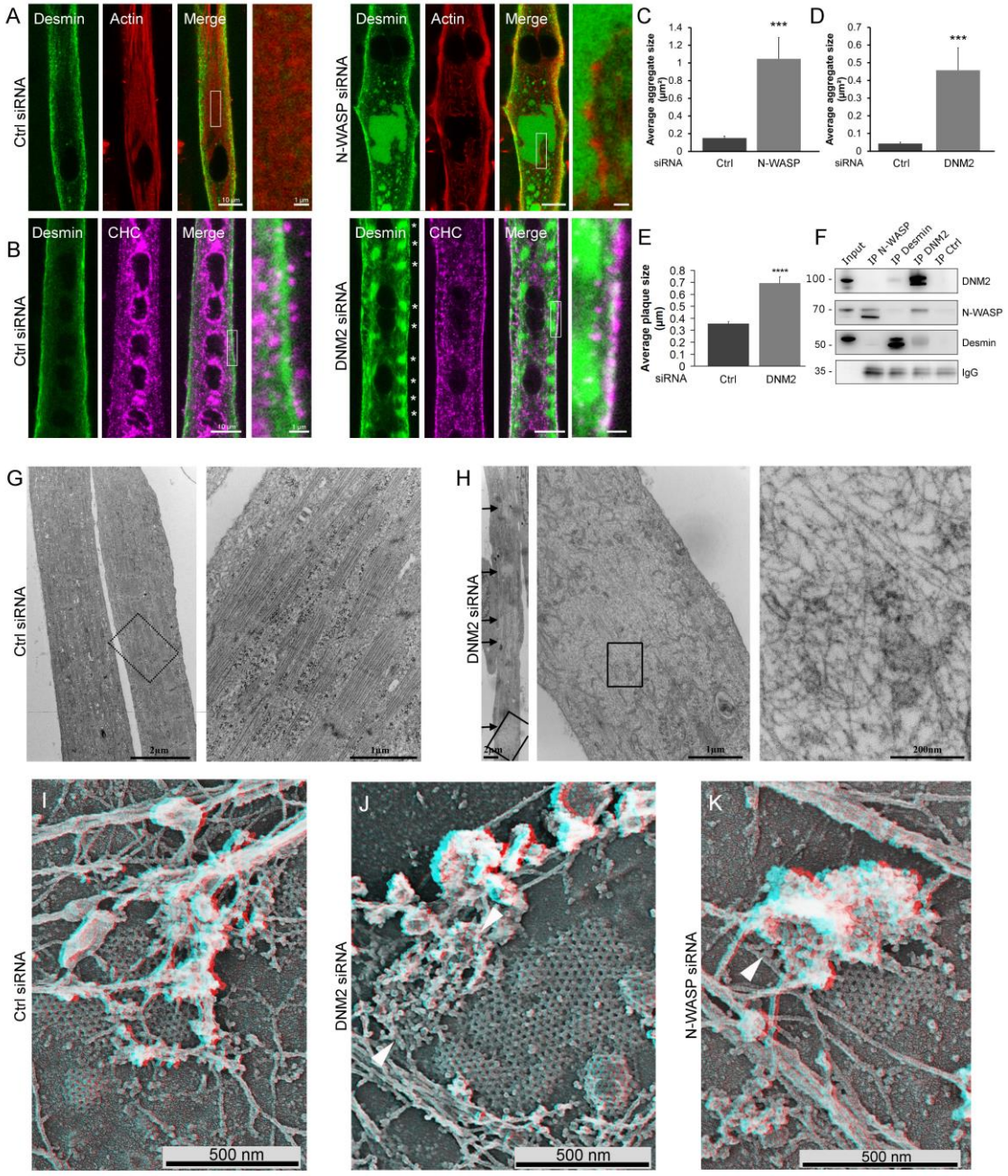

Fig. 2. N-WASP and DNM2 are indispensable for desmin and actin organization around clathrin plaques. (A) Immunofluorescent staining of desmin (green) and actin (red) in mouse primary myotubes treated with control or N-WASP siRNA. **(B)** Immunofluorescent staining of desmin (green) and CHC (magenta) in control or DNM2-depleted mouse primary myotubes. Asterisks denote desmin aggregates aligned along the PM. **(C) (D)** Desmin aggregate fluorescence in myotubes treated with control, N-WASP (C) or DNM2 (D) siRNA (*n* = 20 myotubes). **(E)** Average CCS size in myotubes treated with control or siRNA against DNM2 (*n* = 20 myotubes). **(F)** Immunoblot of proteins associated with N-WASP, desmin, DNM2, or control immunoprecipitates from mouse primary myotubes lysates. **(G) (H)** Thin-section EM of extensively differentiated control (G) or DNM2-depleted (H) myotubes. Arrows denote clearer IF bundles. **(I-K)** High magnification view of unroofed primary mouse myotubes treated with control (I), DNM2 (J) or N-WASP (K) siRNA. Abnormal actin structures are indicated using arrowheads. Use glasses for 3D viewing of anaglyphs (left eye = red). Data are presented as mean ± SEM; *P < 0.05, **P < 0.01, ***P < 0.001, ****P < 0.0001.

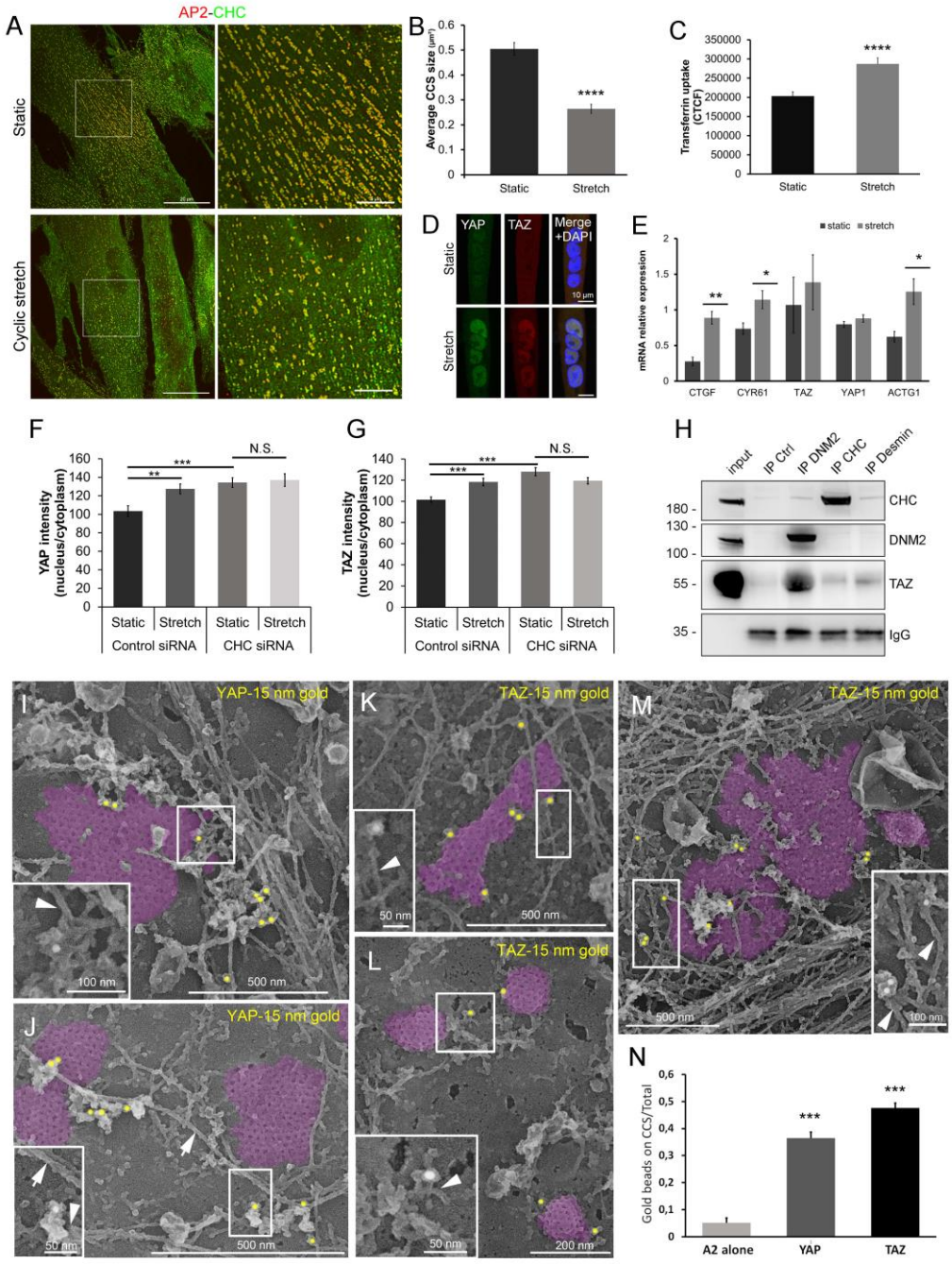

Fig. 3. Clathrin platforms directly sequestrate YAP/TAZ mechanotransducers. (A) Immunofluorescent staining of AP2 (red) and CHC (green) in immortalized human myotubes either stretched or left static. **(B)** Average AP2 patch size in human control myotubes either stretched or left static (n = 20 myotubes). **(C)** Internalized transferrin in human control myotubes either stretched or left static (n = 90–100 myotubes). **(D)** Immunofluorescent staining of YAP (red) or TAZ (green) in primary mouse myotubes stretch or left static. **(E)** Relative expression of YAP/TAZ mRNA target genes (*CTGF, CYR61*) or actin gene *ACTG1* in myotubes stretched or left static (n = 3–4 samples **(F) (G)** YAP or TAZ nucleo/cytoplasmic ratio in control or CHC-depleted myotubes stretch or left static (n = 30–80 myotubes). **(H)** Immunoblot of proteins associated with DNM2, CHC or control immunoprecipitates from human myotube lysates. **(I-M)** High magnification views of clathrin plaques from primary mouse myotubes labelled with YAP (I-J) or TAZ (K-M) antibodies (pseudocolored yellow). Clathrin lattices are highlighted in purple. YAP/TAZ associated to actin cytoskeleton are shown using arrowheads. **(N)** Number of gold beads corresponding to YAP and TAZ labeling on clathrin plaques or surrounding actin cytoskeleton (<100 nm or closer from the clathrin lattice) compared to a staining performed using only secondary antibodies conjugated to 15-nm colloidal gold particles (n = 49 to 104 images). Data presented as mean ± SEM; *P < 0.05, **P < 0.01, ***P < 0.001, ****P < 0.0001.

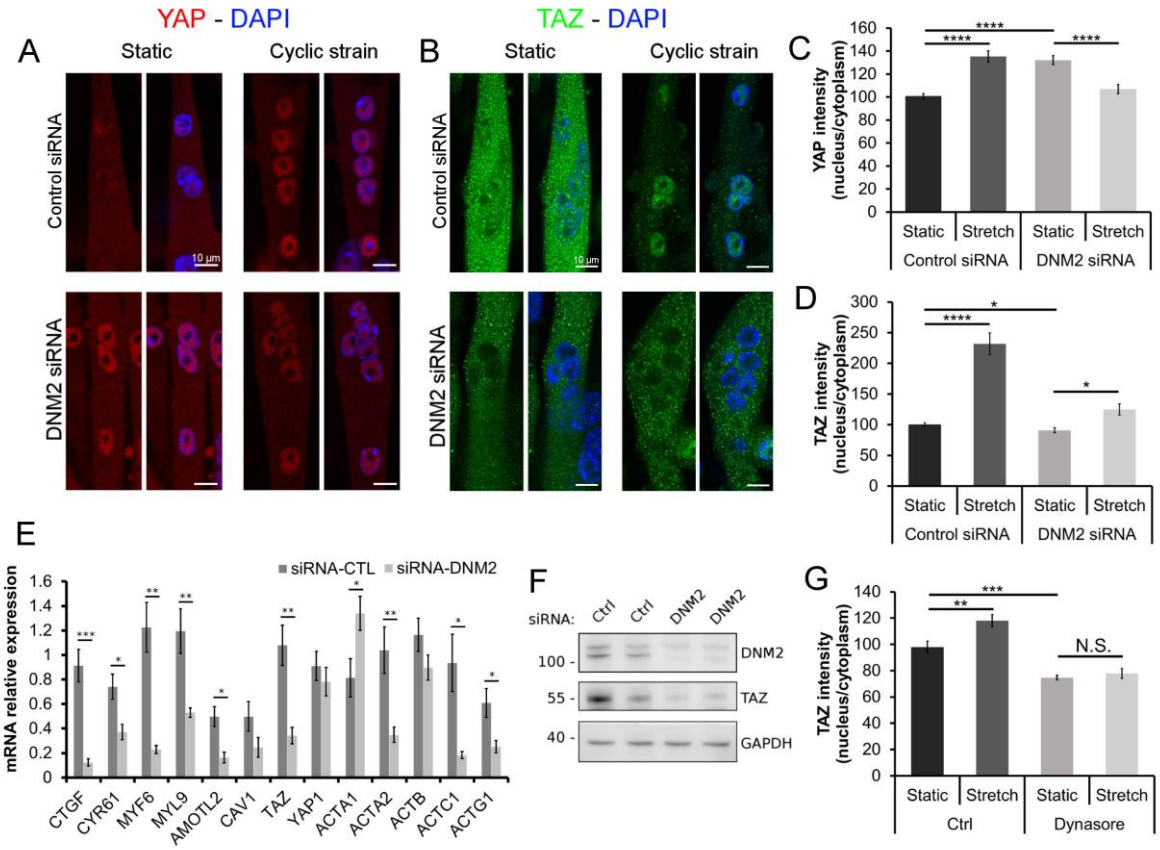

Fig. 4. DNM2 controls YAP/TAZ mechanotransduction in differentiated myotubes. (A) (B) Immunofluorescent staining of YAP (red) or TAZ (green) and nuclei (blue) in mouse primary control or DNM2-depleted myotubes either stretched or left static. **(C) (D)** YAP or TAZ fluorescence in control or DNM2-depleted myotubes (n = 30–45 myotubes). **(E)** Relative expression of YAP/TAZ mRNA target genes or of actin-related genes in control or DNM2-depleted myotubes (n = 6–8 samples). **(F)** Primary mouse myotubes treated with control or DNM2 siRNA and cell lysates immunoblotted for proteins indicated at the right. **(G)** TAZ nucleo/cytoplasmic ratio in human immortalized myotubes treated with or without dynamin inhibitor dynasore and either stretched or left static. Data are presented as mean ± SEM; *P < 0.05, **P < 0.01, ***P < 0.001, ****P < 0.0001.

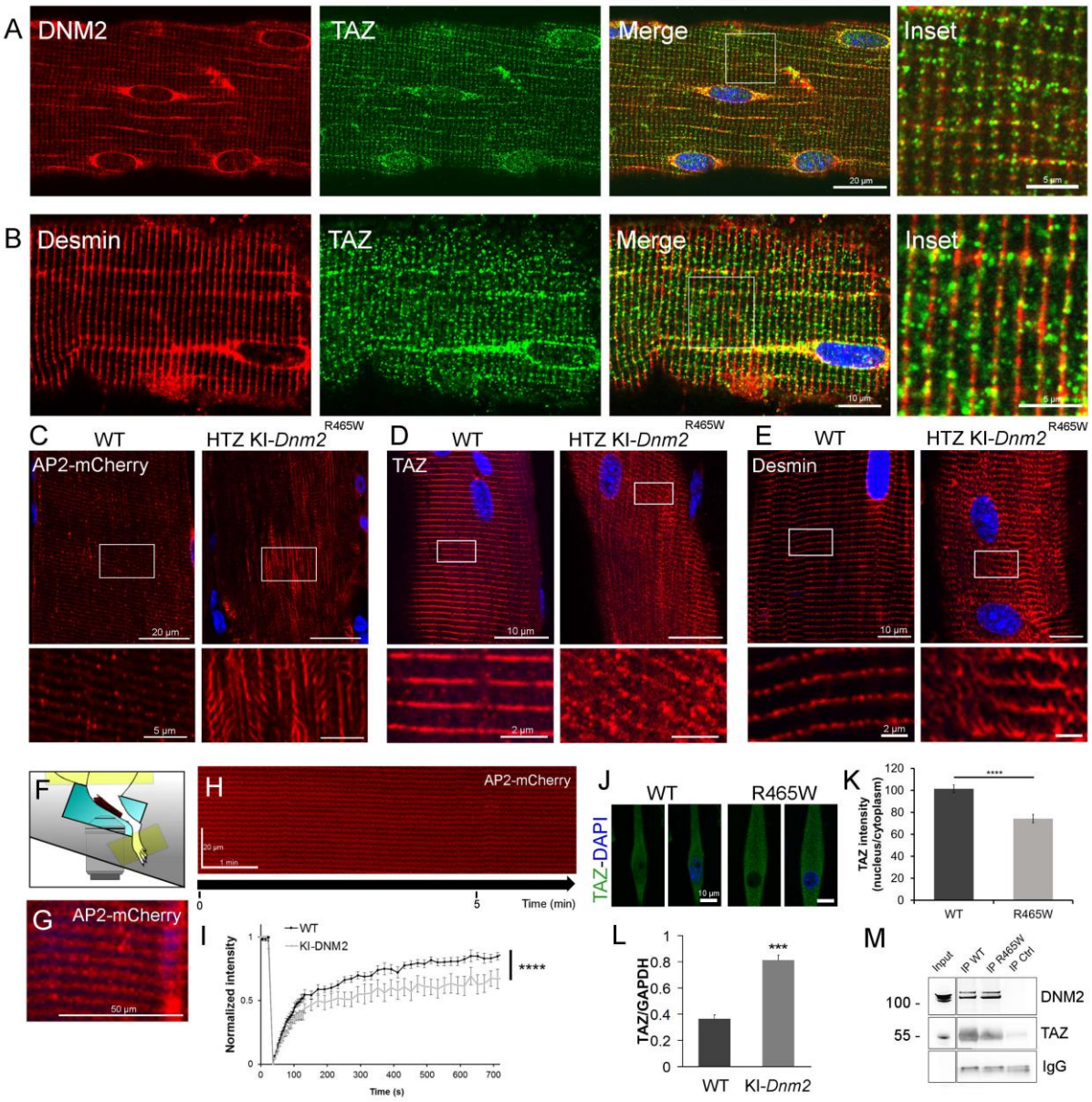

Fig. 5. DNM2-linked CNM mutations delay plaque dynamics and disorganize TAZ and desmin *in vivo*. (A) Immunofluorescent staining of DNM2 (red) and TAZ (green) on isolated mouse TA fibers. Nuclei were stained with DAPI (blue). **(B)** Immunofluorescent staining of desmin (red) and TAZ (green) on isolated mouse TA fibers. Nuclei were stained with DAPI (blue). **(C)** AP2 mCherry distribution between WT and HTZ KI-*Dnm2*^{R465W} mice at the surface of myofibers on longitudinal muscle cryosections. **(D) (E)** Confocal sections from the surface of WT or HTZ KI-*Dnm2*^{R465W} mouse dissociated skeletal muscle fibers immunolabeled with TAZ (D) or desmin (E) antibodies. **(F)** Set-up used to image superficial TA by intra-vital confocal microscopy. **(G)** WT mouse muscle imaged *in vivo*. **(H)** Kymograph of AP2 mCherry fluorescence imaged over 6 minute time-lapse. **(I)** AP2-mCherry fluorescence recovery between WT and HTZ KI-*Dnm2*^{R465W} mice. Two-Way ANOVA was performed, ****P < 0.0001 (n = 17–25 fibers from at least 3 mice for each genotype). **(J)** Immunofluorescent staining of TAZ (green) on primary mouse myotubes from WT or HTZ KI-*Dnm2*^{R465W} mice. **(K)** Nucleo/cytoplasmic ratio of TAZ fluorescence intensity in myotubes from either WT or HTZ KI-*Dnm2*^{R465W} mice (n = 25–30 myotubes). **(L)** Levels of TAZ relative to GAPDH in TA muscle from WT or HTZ KI-Dnm2 R465W mice (n = 4–5 mice per phenotype). **(M)** Immunoblot of TAZ co-immunoprecipitated with DNM2 or control immunoprecipitates from WT or HTZ KI-*Dnm2*^{R465W} primary mouse myotube lysates.

Supplementary material:

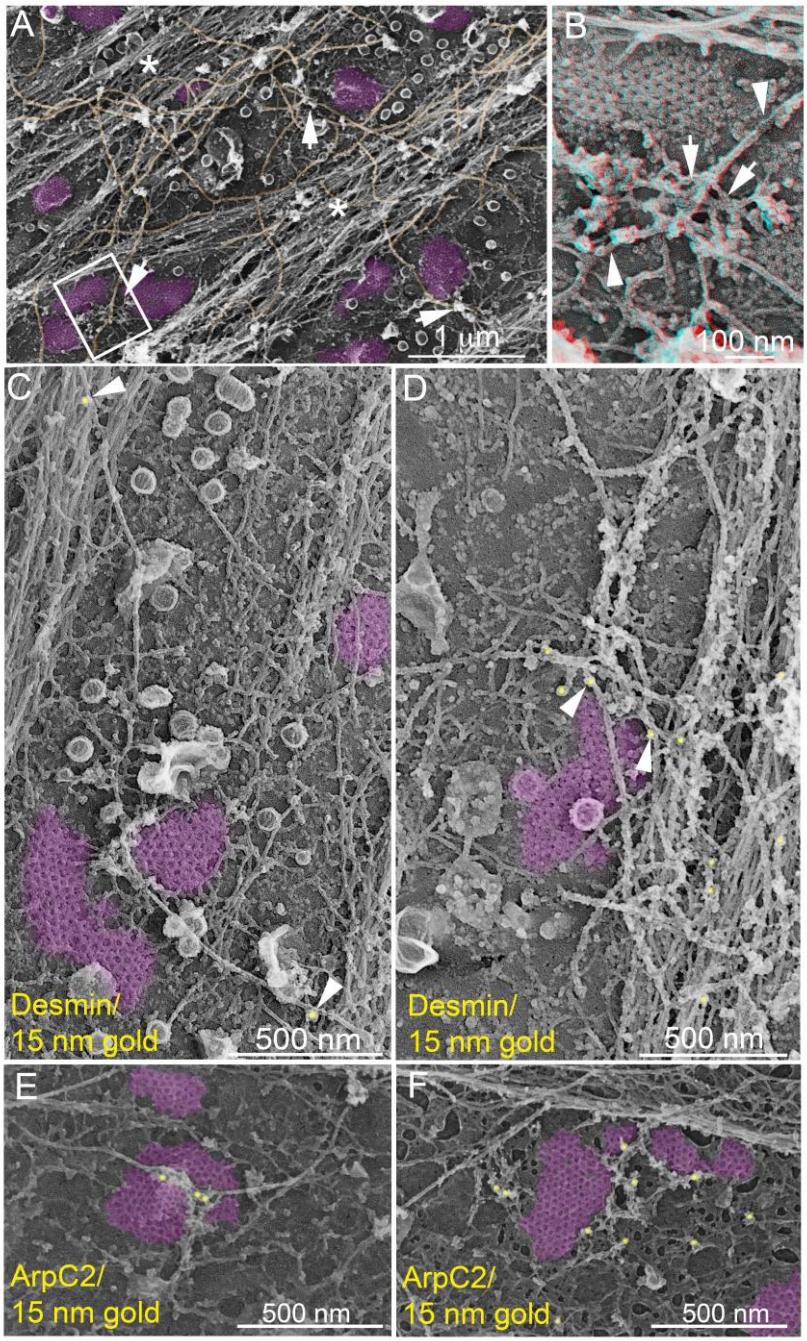

Supplementary Fig. 1. Clathrin lattices anchor desmin intermediate filaments and are surrounded by Arp2/3 branched actin filaments. (A) Survey view of unroofed C2C12 myotubes. Clathrin lattices are highlighted in purple and intermediate filaments in orange. Actin structures around clathrin plaques are indicated with arrows and asterisks denote typical stress fibers. **(B)** 3D anaglyph of the boxed region in (A). Use view glasses for 3D viewing of anaglyphs (left eye = red). Actin network is shown with arrows, while intermediate filaments are indicated with arrowheads. **(C) (D)** Intermediate filaments are immunolabeled using a primary antibody against desmin and secondary antibodies coupled to 15 nm gold beads. Gold beads are pseudocolored yellow and indicated with arrowheads. Clathrin-coated structures are highlighted in purple. **(E) (F)** Branched actin surrounding clathrin plaques is immunolabeled using a primary antibody against ArpC2 and secondary antibodies coupled to 15 nm gold beads. Gold beads are pseudocolored yellow, clathrin lattices are highlighted in purple.

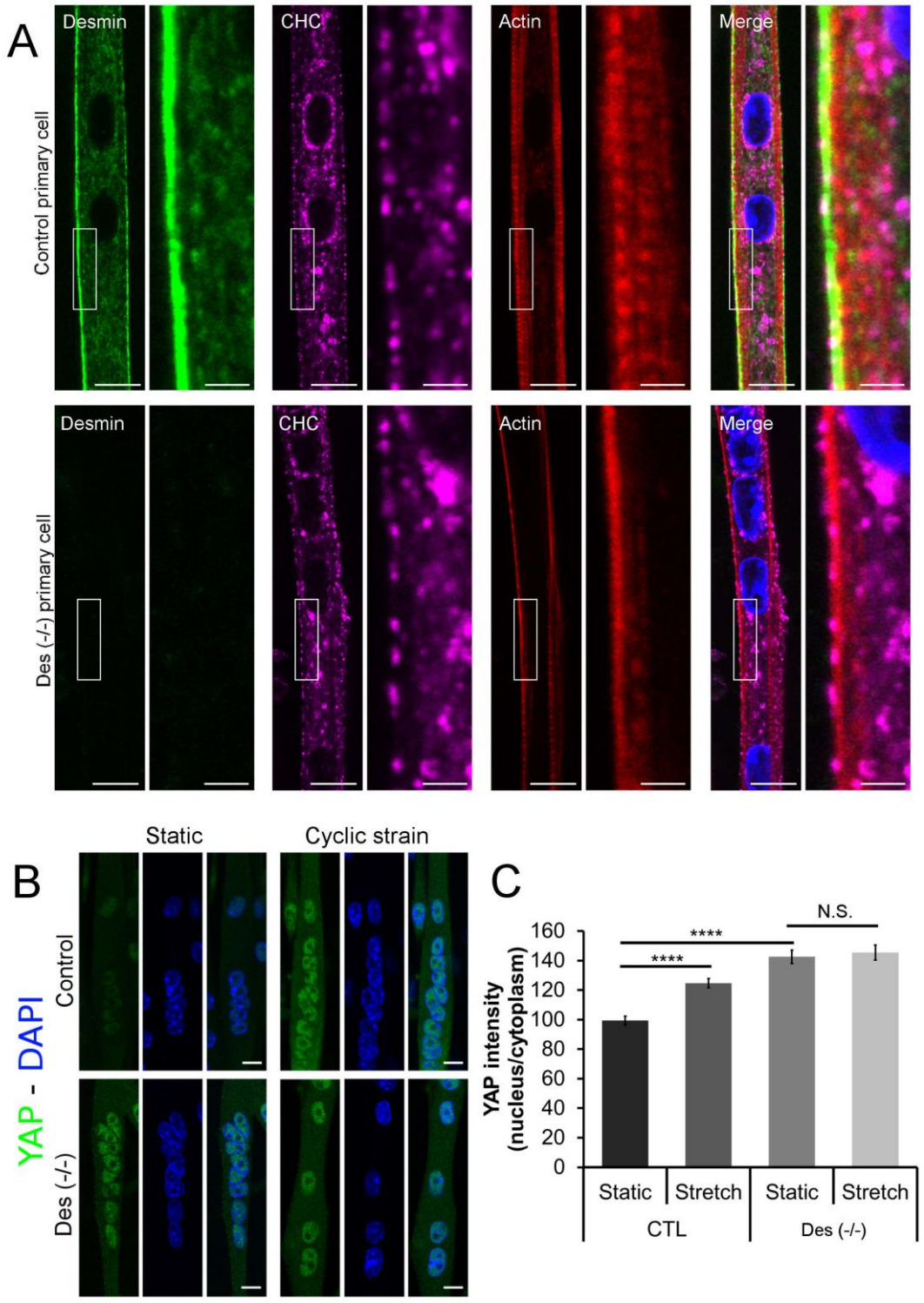

Supplementary Fig. 2. Clathrin plaque presence and increased basal nuclear YAP levels in desmin knock-out mice. (A) Immunofluorescent detection of desmin (green), CHC (magenta) and actin staining (Phalloïdin, red) in differentiated mouse primary myotubes from WT mice (top panel) or myotubes from desmin knock-out mice (Des-/-, bottom panel). Bars 10 µm and 2 µm for insets. **(B)** Immunofluorescent staining of YAP (green) and nuclei (blue) in mouse primary control or Desmin knock-out (Desmin KO) primary myotubes either stretched or left static. **(C)** YAP nucleo/cytoplasmic fluorescence intensity ratio in control or Des-/- myotubes (*n* = 30 myotubes).

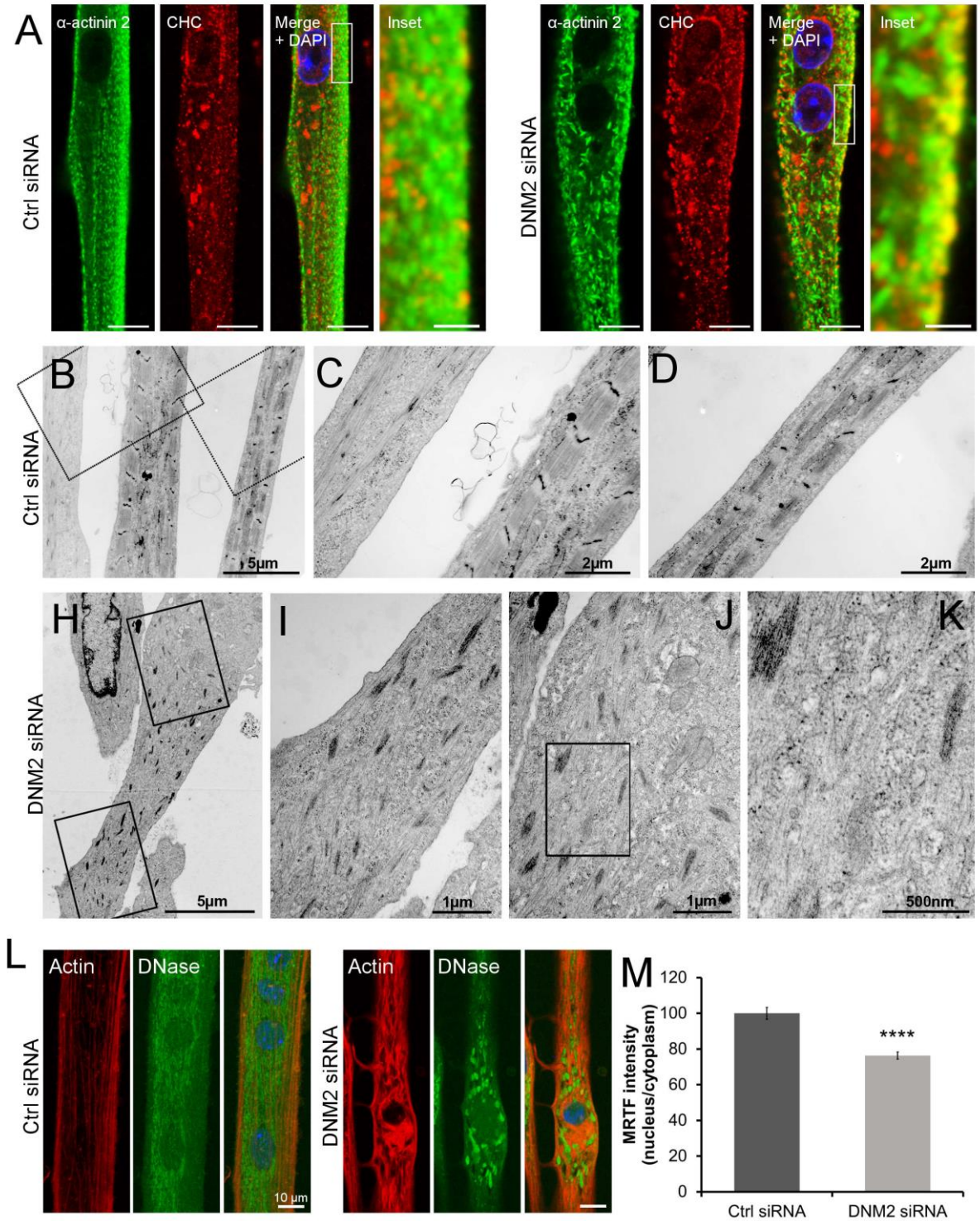

Supplementary Fig. 3. Actin defects in DNM2-depleted myotubes (A) Immunofluorescent staining of α-actinin 2 (green) and CHC (red) in mouse primary myotubes treated with control siRNA or siRNA against DNM2. **(B-K)** Thin-section EM of primary mouse control (B-D) or DNM2-depleted (H-K) myotubes. **(L)** Confocal fluorescent imaging of Alexa Fluor 555 Phalloidin and Deoxyribonuclease I Alexa Fluor 488 conjugate in mouse primary myotubes treated with control or DNM2 siRNA. Nuclei are stained in DAPI. (**M**) Nucleo/cytoplasmic ratio of MRTF in control or DNM2-depleted mouse primary myotubes (n = 22-26 myotubes; Data presented as mean ± SEM; ****P < 0.0001).

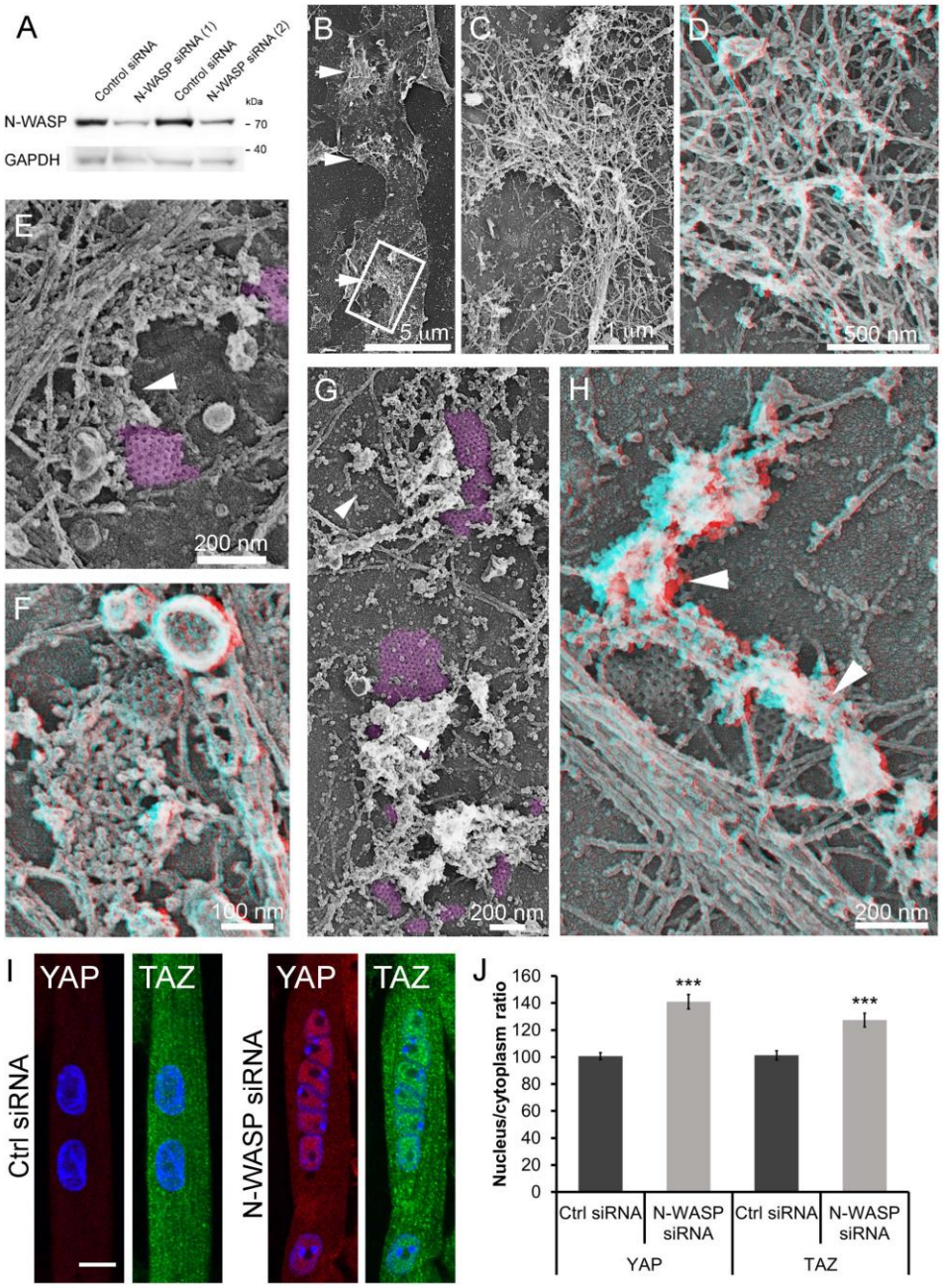

Supplementary Fig. 4. Desmin aggregates, abnormal actin around clathrin plaques and increased nuclear YAP/TAZ basal levels in N-WASP depleted myotubes. (A) Myotubes were treated with control siRNA or two different siRNA targeting N-WASP and cell lysates immunoblotted for proteins (indicated left). **(B)** Survey view of the cytoplasmic surface of the plasma membrane in unroofed primary mouse myotubes treated with siRNA against N-WASP. Arrows indicate the presence of intermediate filament tangles still associated with the PM. **(C) (D)** Higher magnification view of IF tangles associated with the plasma membrane in unroofed primary mouse myotubes treated with siRNA against N-WASP. **(E-H)** Representative branched actin (arrowheads) around clathrin-coated structures (purple) in unroofed primary mouse myotubes treated with siRNA against N-WASP. **(I)** Immunofluorescent staining of YAP (red) or TAZ (green) and nuclei (blue) in mouse primary control or N-WASP depleted myotubes either stretched or left static. Nuclei are stained with DAPI. **(J)** YAP or TAZ fluorescence in control or N-WASP depleted myotubes (n = 30 myotubes). For (D), (F) and (H) use view glasses for 3D viewing of anaglyphs (left eye = red).

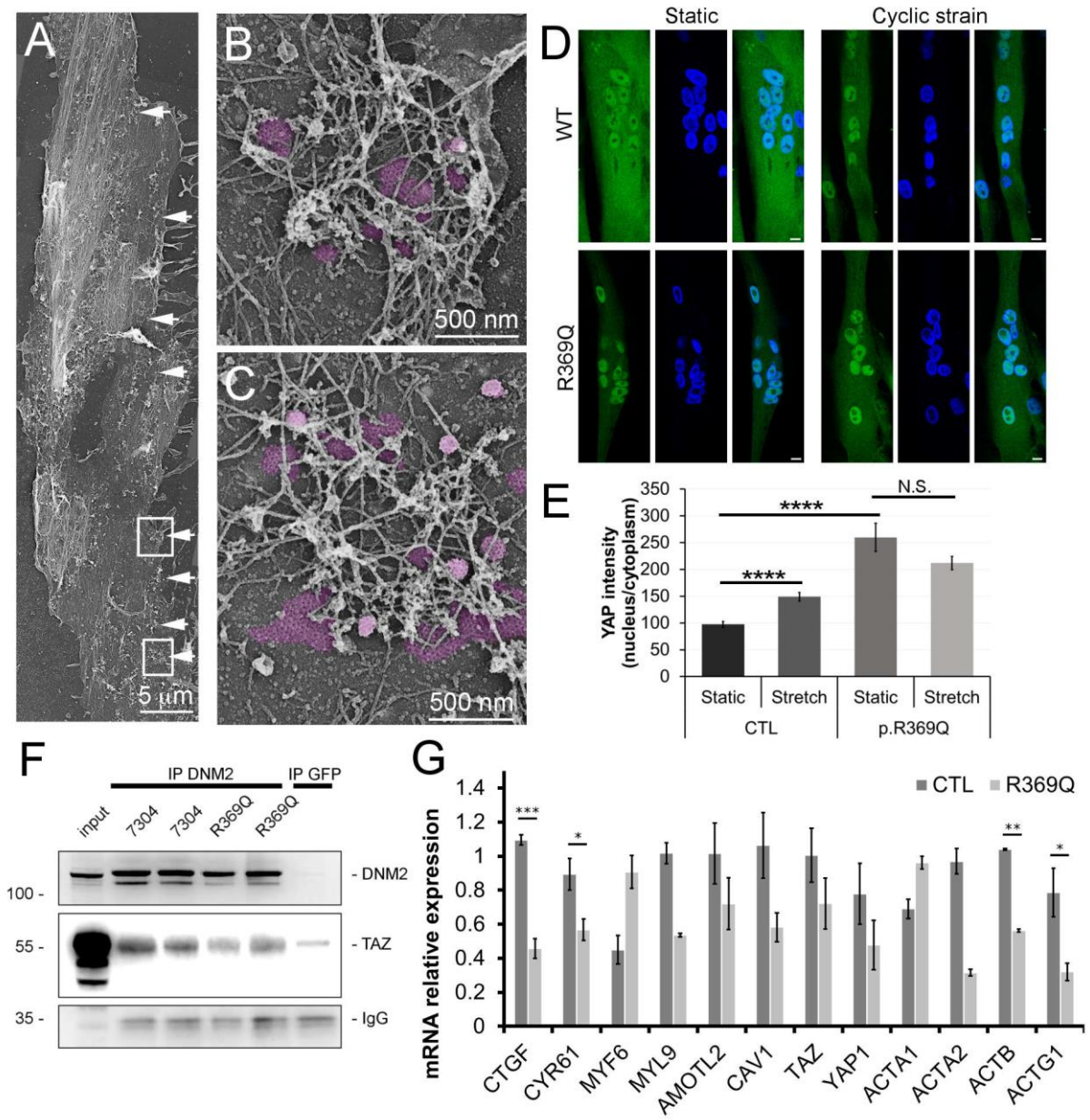

Supplementary Fig. 5. Human myotubes display extensive clathrin-coated plaques and CNM patient myotubes reproduce YAP/TAZ signaling defects. (A) Survey view of the cytoplasmic surface of the PM from an unroofed human myotube. Arrows denote regularly spaced clathrin lattices. **(B) (C)** High magnification views of the boxed regions in (A). Clathrin lattices are pseudocolored in purple. **(D)** Immunofluorescent staining of YAP (green) and nuclei (blue) in control and p.R369Q myotubes either stretched (cyclic strain) or left static. **(E)** YAP fluorescence in control and p.R369Q myotubes either stretched (cyclic strain) or left static. (*n* = 35–60 myotubes). (Data presented as mean ± SEM; ****P < 0.0001). **(F)** Immunoblot of TAZ co-immunoprecipitated with DNM2 or control immunoprecipitates from control or p.R369Q immortalized human myotube lysates. **(G)** Relative mRNA expression of YAP/TAZ target or actin genes in control or p.R369Q myotubes (n = 2–4 samples; Data are presented as mean ± SEM; *P < 0.05, **P < 0.01, ***P < 0.001).

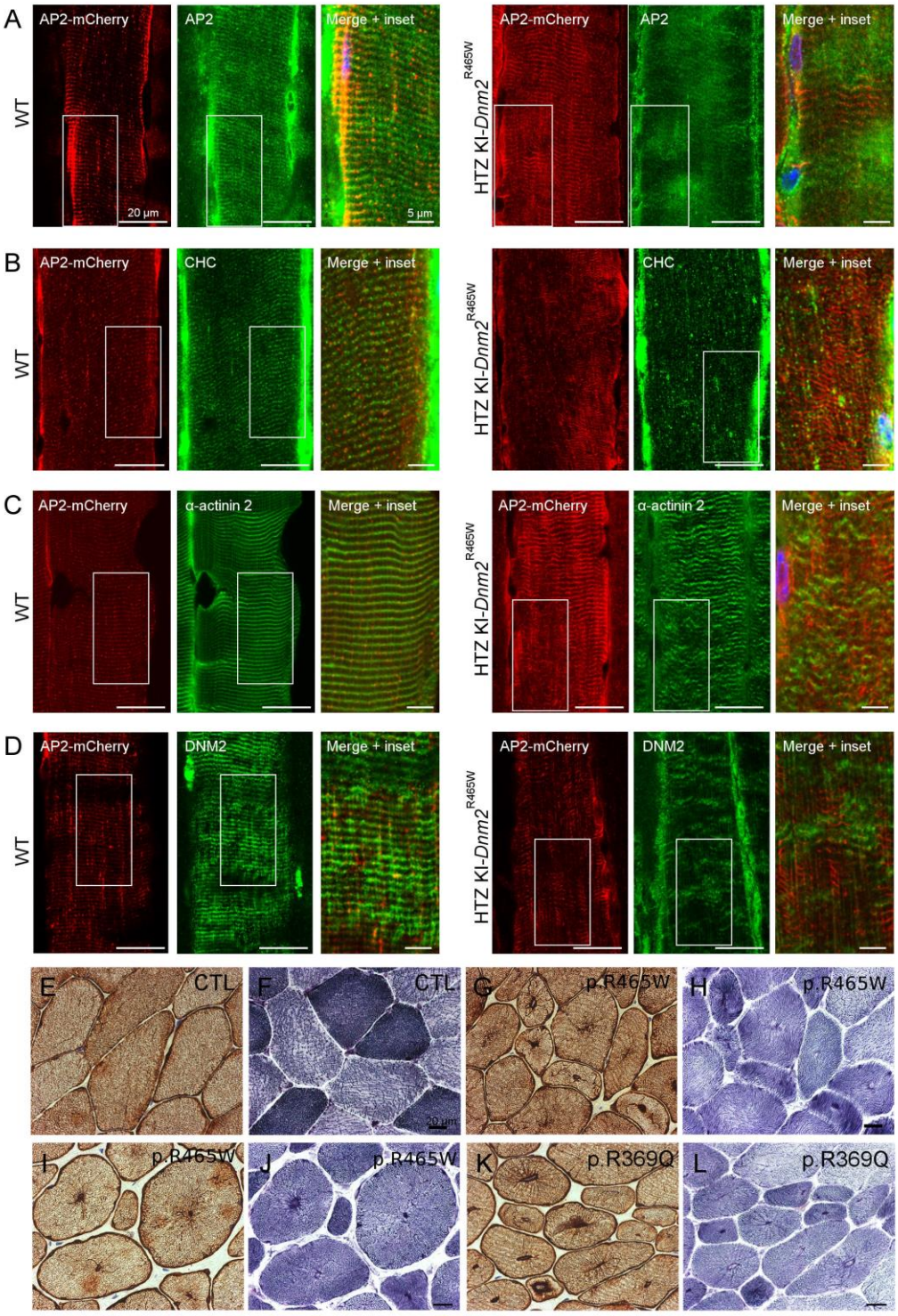

Supplementary Fig. 6. AP2-mCherry localization at skeletal muscle costameres and desmin radial distribution in CNM patients. (A-D) AP2 mCherry distribution between WT (left) and HTZ KI-Dnm2^{R465W} (right) mice on fixed longitudinal muscle sections labelled with antibodies against endogenous AP2 (A), CHC (B), α-actinin 2 (C) or DNM2 (D) respectively. **(E-L)** Biopsy serial sections from one control subject (E-F) and three CNM patients (p.R369Q or p.465W mutation) **(G-L)** immunohistochemical labeling against desmin or NADH-TR reaction. Muscle sections reveal a strong radial sarcoplasmic strand desmin labeling.

Supplementary Table 1. List of primers

	Human primers	
Target	**Forward**	**Reverse**
ACTA1	ACCATGAAGATCAAGATCATCGCCC	CGTCGTACTCCTGCTTGGTGAT
ACTA2	TCCAGCGTTCTGAGCACCCG	GCTGCTTCACAGGATTCCCGTCT
ACTB	AGAGCCTCGCCTTTGCCGAT	ATCATCCATGGTGAGCTGGCGG
ACTC1	CAGCGTTCTATAAAGCGGCCCT	ACCATAACTCCCTGGTGCCG
ACTG1	CCCGCTTCCAGCTGCCGAGG	TCCATTGCGACCCCGCCTTTTGT
AMOTL2	TGACTACAGCAGACAGAGCACCC	TCCCATCTCTGCTCCCGTGTTT
CAV1	CTTCCTTCCTCAGTTCCCTTAAAGCA	GGTGTAGAGATGTCCCTCCGAGT
CTGF	CTGGAAGAGAACATTAAGAAGGGCAA	GCTCGGTATGTCTTCATGCTGG
CYR61	CACGGCCTGTCCGCTGCAC	GGAGAGCGCCAGCCTGGTCA
MYF6	TCGAGTCAGAGGCCAAGGAG	AGGGGGACAAGGTACCATCA
MYL9	CGAATACCTGGAGGGCATGAT	AAACCTGAGGCTTCCTCGTC
TAZ (WWTR1)	CATGGAAGCTGAGACTCTTGCCC	ATATGGCCCTCCATTGAGGAAAGGAT
YAP1	GCTACAGTGTCCCTCGAACC	CCGGTGCATGTGTCTCCTTA
HPRT1	ACCAGTCAACAGGGGACATAAAAGTA	TTTGCCAGTGTCAATTATATCTTCCA
RPLP0	TTCTCGCTTCCTGGAGGGTGT	CGTTGATGATAGAATGGGGTACTGAT
	Mouse primers	
target	**forward**	**reverse**
ACTA1	ACACGCCAGCCTCTGAAACTAGA	TTCACCAGGCCAGAGCCGTT
ACTA2	ATAACCCTTCAGCGTTCAGCCTC	TCTCAGGGTTCCTGACAGCGA
ACTB	CGCGCAGCCACTGTCGAGT	ATCCATGGCGAACTGGTGGCG
ACTC1	AGCTATAAAGCTGCGCTCCAGG	GTGGGTTCTGTAGGCGTGCTAG
ACTG1	ACACTGCGCTTCTTGCCGCT	ACCATGACGCCCTGGTGTCGG
AMOTL2	ACAACACCTCTGCCTGCTTG	GGTTGCAGCTATAGAGTCCAGAGA
CAV1	GGCAAATACGTAGACTCCGAGGGAC	TGTTGCCCTGTTCCCGGATGG
CTGF	TGACCTGGAGGAAAACATTAAGA	AGCCCTGTATGTCTTCACACTG
CYR61	GCACCTTCAGGACGCTCGCT	TGGAGAGCGCCAGTCTGGTC
MYF6	AGAAATTCTTGAGGGTGCGGATT	CACGTTTGCTCCTCCTTCCTT
MYL9	AGGCCTCAGGCTTCATCCA	TCGCGGTACATCTCGTCCA
TAZ (WWTR1)	TTGATCTTGGTGGGAAGAGG	ACGTCTTGCTTGCCTTGTCT
YAP1	AGGGACTCCGAATGCAGTGT	TAGGTGCCACTGTTAAGAAAGGGAT
HPRT1	GTTGGATACAGGCCAGACTTTGTT	AAACGTGATTCAAATCCCTGAAGTA
RPLP0	CTCCAAGCAGATGCAGCAGA	ATAGCCTTGCGCATCATGGT

Supplementary Table 2. List of siRNA sequences

Target	Sequence
CHC	5'-AACAUUGGCUUCAGUACCUUG-3'
DNM2	5'-ACCUACAUCAGGGAGCGAGAA-3'
AP1 (γ-subunit)	5′-AGCUAUGAAUGAUAUAUUA-3′
AP2 (α-subunit)	5′-GAGCAUGUGCACGCUGGCCAGCU-3′
AP3 (δ-subunit)	5′-CAUCAAGAUCAUCAAGCUG-3′
N-WASP (1)	5'-AAUGAAGAAGAAGCAAAAAAGUU-3'
N-WASP (2)	5'-GGAAAUUACUGUGGGAACA-3'

Supplementary Table 3. List of antibodies

Primary antibody (produced in)	Ordered from	Product ref
CHC (rabbit) polyclonal	Abcam	ab21679
DNM2 (rabbit) polyclonal	Abcam	ab3457
AP2 (mouse) monoclonal	Abcam	ab2730
N-WASP (rabbit) polyclonal	Abcam	ab126626
Desmin (mouse) monoclonal	Invitrogen	MA1-06401
Desmin (rabbit) polyclonal	Abcam	ab15200
a-actinin 2 (mouse) monoclonal	Sigma	A7811
p34-Arc/ARPC2 (rabbit) polyclonal	Sigma	07-227
YAP (mouse) monoclonal	Santa Cruz	Sc-101199
TAZ/WWTR1 (rabbit) polyclonal	Sigma	HPA007415
MRTF (mouse) monoclonal	Santa-Cruz	Sc-390324

Supplementary Movie 1. Clathrin structures on the surface of muscle fibers anchor intermediate filaments.

Platinum replica EM with electron tomography by collecting images at the tilt angles up to ±25° relative to the plane of the sample (Supplemental Movies S1). Clathrin lattices are pseudocolored in purple, branched actin in orange and intermediate filaments in green. Image size is 2198 x 885 nm.

Supplementary Movie 2. Persistent clathrin structures on the surface of muscle fibers

Intravital imaging of TA muscle from WT mouse injected with AAV9-AP2 mCherry. Images were captured on a Leica SP8 multiphoton microscope at a frame rate of an image every 690 milliseconds over a 5 min time course. Bar 20 µm.

Supplementary Movie 3. Recovery of AP2 fluorescence in WT mouse.

Intravital imaging of TA muscle from WT mouse injected with AAV9-AP2 mCherry. FRAP was performed after two frames and recovery of fluorescence was recorded several minutes after photobleaching. Time is shown in seconds.

Supplementary Movie 4. Recovery of AP2 fluorescence in HTZ KI-Dnm2^{R465W} mouse.

Intravital imaging of TA muscle from HTZ KI-Dnm2^{R465W} mouse injected with AAV9-AP2 mCherry. FRAP was performed after two frames and recovery of fluorescence was recorded several minutes after photobleaching. Note the abnormal-looking striations of AP2 in KI mouse. Time is shown in seconds.